Key Genetic Determinants Driving Esophageal Squamous Cell Carcinoma Initiation and Immune Evasion

Kyung-Pil Ko,[1] Yuanjian Huang,[1] Shengzhe Zhang,[1] Gengyi Zou,[1] Bongjun Kim,[1] Jie Zhang,[1] Sohee Jun,[1] Cecilia Martin,[2] Karen J. Dunbar,[2] Gizem Efe,[2] Anil K. Rustgi,[2] Hiroshi Nakagawa,[2] Jae-Il Park[1,3,4,*]

[1]Department of Experimental Radiation Oncology, Division of Radiation Oncology, The University of Texas MD Anderson Cancer Center, Houston, TX 77030, USA

[2]Division of Digestive and Liver Diseases, Department of Medicine, Herbert Irving Comprehensive Cancer Center, Columbia University Irving Medical Center, New York, NY 10032, USA

[3]The University of Texas MD Anderson Cancer Center UTHealth Houston Graduate School of Biomedical Sciences, Houston, TX 77030, USA

[4]Program in Genetics and Epigenetics, The University of Texas MD Anderson Cancer Center, Houston, TX 77030, USA

*Correspondence: Jae-Il Park
E-mail: jaeil@mdanderson.org; Tel: 713-792-3659; Fax: 713-794-5369

Disclosure of potential conflicts of interest

No potential conflicts of interest were disclosed.

Author contributions

K.-P.K. and J.-I.P. conceived the experiments. K.-P.K. and J.-I.P. designed the experiments. K.-P.K., Y.H., B.K., S.Z., G.Z., J.Z., and S.J. performed the experiments. K.-P.K., H.N., and J.-I.P. analyzed the data. C.M., K.J.D., G.E., A.-K.R., and H.N. provided ESCC samples. K.-P.K. and J.-I.P. wrote the manuscript.

Data and code availability

Bulk and scRNA-seq data are available via the Gene Expression Omnibus (GEO; GSE213929; log-in token for reviewers: yzcpewsqddwpzcf). The code can be accessed via GitHub (https://github.com/jaeilparklab/ESCC_project_1) and is available upon request.

Acknowledgments

We are grateful to Kwon-Sik Park, Pierre D. McCrea, and Malgorzata Kloc for comments; Ann Sutton (Research Medical Library, MD Anderson) for editing the manuscript; and the Herbert Irving Comprehensive Cancer Center for the shared resources (Biostatistics, Genomics, and Molecular Pathology, and 3D organoid/cell culture). This work was supported by the Cancer Prevention and Research Institute of Texas (RP200315 to J.-I.P.), the National Cancer Institute (CA193297 and CA256207 to J.-I.P; 5P30 CA013696 and 5P01 CA098101 to A.-K.R., H.N., K.D., G.E., C.M.), an Institutional Research Grant (MD Anderson to J.-I.P.), a Specialized Program of Research Excellence (SPORE) grant in endometrial cancer (P50 CA83639), and Radiation Oncology Research Initiatives. The core facilities at Baylor College of Medicine (Cytometry & Cell Sorting Core and Single Cell Genomics Core) were supported by CPRIT (RP180672, RP200504) and the National Institutes of Health (CA125123, RR024574).

Abstract

Background and aims: Despite recent progress in identifying aberrant genetic and epigenetic alterations in esophageal squamous cell carcinoma (ESCC), the mechanism of ESCC initiation remains unknown.

Methods: Using CRISPR/Cas 9-based genetic ablation, we targeted 9 genes (*TP53*, *CDKN2A*, *NOTCH1*, *NOTCH3*, *KMT2D*, *KMT2C*, *FAT1*, *FAT4*, and *AJUBA*) in murine esophageal organoids (EOs). Transcriptomic phenotypes of organoids and chemokine released by organoids were analyzed by single-cell RNA sequencing (scRNA-seq). Tumorigenicity and immune evasion of organoids were monitored by allograft transplantation. Human ESCC scRNA-seq datasets were analyzed to classify patients and find subsets relevant to organoid models and immune evasion.

Results: We established 32 genetically engineered EOs and identified key genetic determinants that drive ESCC initiation. A single-cell transcriptomic analysis uncovered that *Trp53*, *Cdkn2a*, and *Notch1* (PCN) triple-knockout (KO) induces neoplastic features of ESCC by generating cell lineage heterogeneity and high cell plasticity. *PCN* KO also generates an immunosuppressive niche enriched with exhausted T cells and M2 macrophages via the CCL2-CCR2 axis. Mechanistically, *CDKN2A* inactivation transactivates *CCL2* via NF-κB. Moreover, comparative single-cell transcriptomic analyses stratified ESCC patients and identified a specific subtype recapitulating the PCN-type ESCC signatures, including the high expression of CCL2 and CD274/PD-L1.

Conclusions: Our study unveils that loss of *TP53*, *CDKN2A*, and *NOTCH1* induces esophageal neoplasia and immune evasion for ESCC initiation and proposes the CCL2 blockade as a viable option for targeting PCN-type ESCC.

Keywords: Esophageal squamous cell cancer, CCL2, organoids, immune evasion, single-cell RNA-sequencing, TP53, CDKN2A, NOTCH, patient stratification, immunotherapy

Introduction

ESCC accounts for over 80% of all esophageal cancer cases and has a poor prognosis because of a lack of symptoms in the early stages. The 5-year overall survival rate of patients with esophageal cancer ranges from 10% to 25%.[1] ESCC develops from squamous dysplasia and is asymptomatic until it spreads to other tissues,[2] which leads to late detection. Therefore, understanding the mechanisms of esophageal neoplasia and ESCC initiation is imperative to improving the detection, diagnosis, treatment, and prevention of ESCC. However, despite a recent genome-wide analysis of ESCC patients, the key genetic factors that drive ESCC neoplasia and initiation remain elusive.

In addition to the genetic and epigenetic alteration of tumor cells, the tumor microenvironment (TME)[3] plays a pivotal role in tumorigenesis. The TME comprising immune and stromal cells surrounding tumor cells designs the immune landscape to elicit immunosuppressive effects on tumors and various immunotherapeutic responses.[4, 5] Although the TME's effects on tumor cells are biphasic, as immune cells generally recognize tumor cells or neoantigens to generate anti-tumor immune responses,[6] the tumor-favorable TME induces tumor growth, invasion, and metastasis.[7] The TME is also an indispensable factor in ESCC development, as it provides drug resistance and immunosuppressive immune cell infiltration.[8, 9]

Immune checkpoint inhibitors (ICIs) have been clinically tested in ESCC patients and have shown promising results.[10-14] However, not all patients benefit from ICIs, alone or in combination with first-line therapy,[8] possibly because of the lack of a clear classification of ESCC patients. The underlying genetic background of immunosuppressive microenvironment has yet to be identified. Herein, we found that the genetic inactivation of *TP53*, *CDKN2A*, and *NOTCH1* induces esophageal neoplasia (cell-autonomous) and generates an immunosuppressive niche (non-cell-autonomous) to promote ESCC tumorigenesis.

Methods

Mice

C57BL/6, *Trp53*$^{floxed/floxed}$ (JAX no. 008462) and *Rosa26nT-nG* (JAX no. 023035) mice purchased from the Jackson Laboratory were bred and housed in the Animal facility at MD Anderson Cancer Center on a 12-hr light/dark cycle. All animal procedures were performed according to the guidelines of the Association for the Assessment and Accreditation of Laboratory Animal Care and institutionally approved protocols. The study was compliant with all relevant ethical regulations regarding animal research.

Wnt3A, R-Spondin1, and Noggin-Conditioned Medium

The Wnt3A, R-Spondin1, and Noggin (WRN)-conditioned medium was prepared as previously described.[15] In brief, L-WRN (ATCC CRL-3276) cells were cultured on a 10-cm plate with culture medium (Dulbecco's modified Eagle's medium [DMEM, Fisher], 0.5 mg/mL G418 (Thermofisher), 0.5 mg/mL hygromycin B (Thermofisher), 1% penicillin/streptomycin (Life Technologies), and 10% fetal bovine serum). After 10% of L-WRL cells (ATCC, CRL-3276) had been seeded in culture medium (without G418 and hygromycin B) in 10-cm plates, cells were incubated for 3-4 days. The medium was replaced with 10 mL of fresh medium when the cells were 80%-90% confluent, and the cells were incubated for 24 hrs. The medium was collected, centrifuged at 1000 $\times$ g for 4 min, passed through a 0.22-μm sterile filter, and stored at −80 °C. Another 10 mL of fresh medium was added to the plates and collected after 24 hrs to make the second batch of conditioned medium using the same procedures. The first, second, and third batches of conditioned media were mixed before use to prepare a 100% WRN-conditioned medium.

Esophageal Tissue Isolation

Tissues were collected from mice (8~10-week-old) euthanized via CO_2 inhalation followed by cervical dislocation. The esophagi were collected in 10-cm Petri dishes with ice-cold phosphate-buffered saline (PBS) with 1% penicillin/streptomycin and swirled gently to remove blood. The esophagi were opened longitudinally and washed with cold

PBS. The epithelial cell layer was peeled off using surgical tweezers and then dissected into 0.5-cm^3 pieces with surgical blades. The minced esophagi were collected in a 15-mL conical tube and digested by 0.05% trypsin-EDTA (Thermofisher) at 37 □ for 60 min with frequent vortexing. After dissociation, 3× volume 10% fetal bovine serum-supplemented DMEM was added, followed by vigorous pipetting. The suspension was passed through a 35-μm cell strainer to collect a single-cell suspension. Finally, the cell suspension was spun down at 1000 rpm for 4 min and resuspended in a 50% WRN-conditioned medium.

EO Culture

The E-MEOM was used to culture EOs. Single-cell–dissociated esophageal epithelial cells (1000 cells) were suspended in 8 μL of E-MEOM and 12 μL of pre-thawed Matrigel (Corning) on ice and seeded in the centers of a well to create a Matrigel dome. The plate was incubated at 37 °C for 10 min to solidify the Matrigel. Finally, 500 μL of E-MEOM was added and incubated at 37 °C with 5% CO_2. The medium was changed every 2-3 days.

***Trp53KO* EO**

Esophagi from 8- to 10-week-old *Trp53*$^{floxed/floxed}$ mice were digested into a single-cell suspension and seeded in Matrigel to form EOs, as described above. After 7 days of culture, EOs were digested with 0.05% trypsin-EDTA at 37 °C for 45 min to create a single-cell suspension. Ad-CMV-EGFP or Ad-Cre-EGFP (University of Iowa) was added to the cell suspension at 1×10^3 pfu/cell. Cells were then suspended in Matrigel to generate new EOs. After 2 days of seeding, 10 μM nutlin3 was added for *Trp53*$^{floxed/floxed}$ cell selection. Two days later, the selection was performed by sorting the GFP+ cells after dissociating EOs into single cells, and the sorted cells were re-seeded for EO culture, as described above. EOs were collected for genotyping 7 days after seeding. Wild-type, *Trp53*$^{floxed/floxed}$, and KO Trp53 alleles were amplified as 288 bp, 370 bp, and 612 bp, respectively. See Supplementary Table 1 for primer information.

CRISPR/Cas9-Based Gene Targeting in EOs

CRISPR/Cas9 system-mediated gene KO was described in a previous study.[16] In brief, WT or *Trp53* KO EOs were digested with 0.05% trypsin-EDTA to dissociate into single cells. Single cells were incubated with a virus-containing medium with polybrene for 1 hr with centrifugation (600 g) at 32 °C (see Supplementary Table 2 for sgRNA sequences). Cells were then incubated at 37 °C with 5% CO_2 for 4 more hrs and embedded in Matrigel. The medium was replaced 2 days after infection with antibiotics (puromycin [Sigma], blasticidin [Invitrogen], or hygromycin) for selection. Gene KO was confirmed by genomic DNA PCR (see Supplementary Table 1 for primer information). Additional details are described in the Supplementary Methods.

Results

Genetic ablation of *Trp53* and *Notch1* is sufficient to induce esophageal neoplasia

To elucidate the vital genetic events initiating ESCC, we analyzed genetic alterations in ESCC patients (*n* = 86). Recurrent loss-of-function mutations in *TP53*, *CDKN2A*, *KMT2D*, *KMT2C*, *FAT1*, *FAT4*, *AJUBA*, *NOTCH1*, and *NOTCH3* genes were observed in ESCC patients.[17, 18] The *TP53* and *CDKN2A* genes were the most commonly altered (> 70%) (Figure S1A). More than 50% of mutations in the *CDKN2A*, *KMT2D*, *NOTCH1*, and *FAT1* genes were frameshift or truncation mutations (Figure S1B). Additionally, ESCC patients displayed transcriptional downregulation of *KMT2C* and *FAT4* genes (Figure S1C). To understand the significance of the nine genes (*TP53*, *CDKN2A*, *KMT2D*, *KMT2C*, *NOTCH1*, *NOTCH3*, *FAT1*, *FAT4*, and *AJUBA*) in ESCC initiation, we tested the functional impact of their inactivation on the transformation of esophageal organoids (EOs), as recently established (Figure 1A, S2A).[19, 20] Employing the CRISPR system, we genetically ablated the nine genes in 32 different combinations. Given that *TP53* and *CDKN2A* genes were the most frequently mutated, *Trp53* KO and *Cdkn2a* KO were chosen as the foundation for additional gene ablations, and double KO (dKO) or triple KO (tKO) EOs were established (Figure S1D-F, S2B,C).

Combined with *Trp53* and *Cdkn2a* dKO, genetic ablation of *Notch1*, *Fat4*, or *Ajuba* resulted in markedly increased EO size (Figure 1B). However, only *Notch1* KO with *Trp53* and *Cdkn2a* dKO EOs displayed cell differentiation (central keratin pulp) loss and hyperplastic growth simultaneously (Figure 1B and C). KO of *Ajuba* or *Fat4* with *Trp53* or *Cdkn2a* dKO was insufficient to induce neoplastic transformation, as these cells showed keratin pulp (well-differentiated). *Notch1* KO induced loss of keratin layer at the center of organoids, regardless of *Trp53* and *Cdkn2a* status, indicating a major role of NOTCH signaling in esophageal epithelial cell differentiation (Figure 1C). The increased number of proliferating cells was confirmed by MKI67 staining in dKO of *Trp53* and *Notch1* (PN) and tKO of *Trp53*, *Cdkn2a*, and *Notch1* (PCN) EOs (Figure

1D,E, S3A). Compared to other EOs, PN and PCN EOs showed upregulated expression of ESCC stemness markers (Sox2 and Trp63) and increased cell proliferation (Figure 1D-H, S3A). *Notch1* KO suppressed organoid cell differentiation, as represented by decreased Krt13, a cell differentiation marker (Figure 1F, S3B-D).

Since ESCC invades stromal cell layers at an early stage,[21, 22] we analyzed EO cell invasiveness by co-culturing EOs on the stromal cell layer. While WT EO-derived epithelial cells formed distinct epithelial cell colonies, PN and PCN EO-derived cells were mixed with a stromal cell layer (Figure 1I,J, S3E), recapitulating ESCC's invasive feature. We further examined the tumorigenicity of each group of EOs in 2D culture by assessing cell growth without supporting materials and growth factors in the organoid culture system. In 2D culture, only PN and PCN EOs showed increased colony formation, exponential cell growth, and cell migration, whereas PCA and PCF4 organoids showing increased size in 3D culture did not proliferate without the supporting factors (Figure S3H). Notably, PN EOs showed relatively faster growth than did PCN EOs (Figure 1K,L, S3F,G). Additionally, AB-PAS staining showed that PN and PCN EOs did not express mucins highly expressed in esophageal adenocarcinoma (EAC), indicating that PN- and PCN-induced neoplasia is unrelated to EAC (Figure S3I). Furthermore, since the upper esophageal cells were the source of the organoids, it is inherently unlikely that EAC development would occur. These results suggest that *Trp53* and *Notch1* dKO (PN) and *Trp53*, *Cdkn2a*, and *Notch1* tKO (PCN) are sufficient to induce neoplastic transformation that exhibits the characteristics of early-stage ESCC.

Dysregulated cell plasticity and lineage trajectories of neoplastic EOs

Next, to understand the mechanism of ESCC initiation, we performed multiplexed single-cell RNA-sequencing (scRNA-seq) of WT, PC, PN, and PCN EOs (Figure 2A-C, S4A). Thirty-five cell clusters were annotated with multiple markers that are specifically expressed in proliferative (*Mki67*, *Top2a*, and *Stmn1*), early suprabasal (*Ptma*, *Itgb4*, and *Krt5*), intermediate suprabasal (*Itga6*), and stratified (*Krt13*, *Krt4*, and *Sprr3*) cell

types (Figure S4B-D).[19, 23] The intermediate suprabasal cell cluster showed a moderate expression level of early suprabasal markers (*Itgb4* and *Krt5*) and stratified markers. The proliferative cells were significantly enriched in the PC, PN, and PCN organoids compared to in the WT EOs mainly composed of differentiated (stratified and suprabasal) cells (Figure 2D, S4E), recapitulating EO phenotypes (Figure 1).

Having observed distinct cell hyperproliferation and de-differentiation by PN and PCN, we performed RNA velocity-based cell lineage trajectory inference (Figure 2E). Intriguingly, PN and PCN showed multiple root cell clusters (PN3, PN4, PN8 and PCN3, PCN4, and PCN7, respectively), whereas WT harbored a single root cell cluster (WT4), also reproduced in the latent time and PAGA analyses (Figure 2F-I). These results imply that *Trp53* and *Notch1* dKO might generate distinct cellular plasticity and higher cellular heterogeneity.[24]

Human ESCC features in *Trp53*/*Notch1* dKO and *Trp53*/*Cdkn2a*/*Notch1* tKO EOs

We assessed the pathological relevance of genetically engineered EOs to human ESCC by comparing their transcriptional signatures. Compared to WT and PC EOs, ESCC cancer stem cell markers, including *Trp63*, *Krt5*, and *Tfrc*, were intensively enriched in the proliferating cells of PN and PCN EOs (Figure 3A). *Sox2* and *Gnl3* were highly expressed in the proliferating cells of PN and PCN EOs, respectively, while the other genes did not show specificity to the PN or PCN cell types. We also compared the transcriptional features of our EOs with those of ESCC patients from the TCGA database using the Scissor (v2.0.0) package. The gene expression feature comparison analysis showed the similarity of each EO to ESCC patients: WT (35.4%), PC (52.2%), PN (50.5%), and PCN (52.2%) (Figure 3B,C). In addition, PCN (21.9%) showed the highest similarity with the poor survival–associated ESCC patients compared to the other organoids (Figure 3D,E). A gene set enrichment analysis further confirmed that the PCN-highly expressed gene set was enriched in ESCC-specific gene features, while the PN-highly expressed gene set enrichment was not statistically significant (Figure

3F). To increase the sequencing read depth, we also performed bulk RNA-seq of WT, PN, and PCN EOs and reanalyzed the gene expression of each dataset (Figure 3G). Using the differentially expressed genes (DEGs) of PN to WT or PCN to WT, we ran the Enrichr analysis with PN or PCN highly expressed genes. Both PN and PCN highly expressed genes were enriched with features of the cell cycle, DNA replication, and mitotic cells in the Bioplanet and REACTOME databases (Figure 3H). The “pathways in cancer” were also associated with the PCN highly expressed genes in the Kyoto Encyclopedia of Genes and Genomes (KEGG) pathway enrichment analysis (Figure 3I). These results suggest that the transcriptomic patterns of human ESCC are most similar to the transcriptomic features of *Trp53*, *Cdkn2a*, and *Notch1* tKO EOs.

***Trp53*/*Cdkn2a*/*Notch1* tKO cells are tumorigenic *in vivo* via CCL2-mediated immune evasion**

Having determined that either PN dKO or PCN tKO is sufficient to induce the neoplastic phenotype *in vitro* (Figures 1, 2), we determined their impact on ESCC tumorigenesis *in vivo* by congenic transplantation. Subcutaneously injected PN and PCN cells developed tumors in immunocompromised mice (Figure S5A-E), consistent with the *in vitro* results. However, in immunocompetent mice, only PCN cells exhibited tumor growth, with a success rate of 60%, whereas PN cells failed to proliferate (0 of 5) (Figure 4A,B). This finding was intriguing, as it was unexpected given the superior growth rate of PN cells compared to that of PCN cells *in vitro* (Figure 1K,L). PCN cell–derived tumors had substantially invaded the muscular layer with poorly differentiated squamous cell carcinoma (Figure 4B). PCN tumors were hyperproliferative, with ESCC stemness marker (SOX2, TRP63) expression, recapitulating the features of ESCC (Figure 4C).

These results led us to hypothesize that PCN cells evade immune surveillance, while PN cells do not. Indeed, $CD4^+$ T cells, $CD8^+$ T cells, neutrophils, and dendritic cells infiltrated the PCN-derived tumors, implying an active interaction between tumor and immune cells (Figure S5F). To test this, we comparatively examined PN and PCN

transcriptomes. An Enrichr analysis showed that the genes associated with T-cell receptor signaling and antigen processing and presentation were highly enriched in the PCN compared to in the PN (Figure S5G). A DEG analysis of bulk RNA-seq showed that the genes related to immune response and cytokine-related signaling pathways were highly expressed in PCN compared to in PN (Figure 4D, S5H), suggesting that cytokines or chemokines specifically expressed in PCN cells contribute to immune evasion. A comparative DEG analysis of scRNA-seq datasets identified three cytokines (*Ccl2*, *Cxcl1*, and *Cxcl2*) highly upregulated in PCN (Figure 4E). Notably, only *Ccl2* expression was enriched explicitly in the PCN compared to in WT, PC, and PN (Figure 4F, S5I-M), validated by immunostaining of PCN allograft tumors for CCL2 and its receptor, CCR2 (Figure S5N).

Since CCL2 expressed by tumor cells recruits myeloid cells (monocytes, tumor-associated macrophages [TAMs], and myeloid-derived suppressor cells [MDSCs]) to the TME, inhibiting the CCL2-CCR2 axis was shown to enhance the immune response to tumors.[25-28] To determine the role of Ccl2 in immune evasion of PCN cells, we genetically ablated the *Ccl2* gene in PCN cells (PCN-*Ccl2* KO) and compared the tumorigenicity of PCN and PCN-*Ccl2* KO cells using allograft transplantation. PCN and PCN-*Ccl2* KO showed no difference in cell growth *in vitro* (Figure S6A,B) or tumor growth in immunocompromised mice (Figure S6C,D). However, unlike PCN cells, PCN-*Ccl2* KO cells barely developed tumors in immunocompetent mice (Figure 4G-I). Although immune cells were abundant in both PCN parental and *Ccl2* KO tumors, the keratin pearls, one of the signatures of ESCC, were mainly observed in PCN tumors compared to in *Ccl2* KO tumors, indicating that PCN tumors develop with less interruption by immune cells (Figure S6E). In line with this, the number of exhausted T (T_{ex}) cells (expressing Pdcd1/Pd-1) was increased among the immune cells surrounding PCN tumors compared to those surrounding PCN-*Ccl2* KO tumors (Figure 4J,K, S6F). Moreover, PCN-*Ccl2* KO tumors showed a higher number of cells with perforin, an effector $CD8^+$ T cell marker, $CD8^+$ T cells, and cleaved-Caspase-3^+ (an apoptotic cell marker) cells compared to PCN tumors, suggesting that more cell death mediated by T cells occurs in PCN-*Ccl2* KO tumors than in PCN tumors (Figure 4J,K, S6G).

Simultaneously, a more significant number of $CD206^+$ (an M2 macrophage marker) cells was observed in PCN tumors than in PCN-*Ccl2* KO tumors (Figure 4J,K, S6F).

Although we found fewer M2 macrophage marker–expressing cells in PCN-*Ccl2* KO tumors than in PCN tumors, we did not find significant differences in the number of infiltrating M1 macrophages ($CD68^+$/$CD80^+$ cells) or MDSCs ($CD11B^+$/$LY6G^+$ cells) (Figure S6F-H). Nonetheless, the proliferation of PCN and PCN-*Ccl2* KO tumors was comparable based on the $MKI67^+$ cell quantification (Figure 4J,K, S6F). These results suggest that CCL2 secreted from PCN tKO tumor cells contributes to immune evasion in ESCC tumorigenesis.

Emerging CCL2-CCR2 interaction between tumor and immune cells during ESCC tumorigenesis

To complement allograft models, we analyzed single-cell transcriptomics of an autochthonous mouse model.[29] In this model, treatment of 4-NQO (4-nitroquinoline 1-oxide) resulted in the development of inflammation, hyperplasia, dysplasia, cancer in situ, and invasive cancer in the esophageal epithelium in a time-dependent manner. From the scRNA-seq datasets of the 4-NQO model, the epithelial cells (proliferating, basal, suprabasal, stratified, and other cells) and the immune cells were sub-clustered based on marker gene expression (Figure S7A-F). This ESCC model showed decreased expression of Trp53, Cdkn2a, and Notch signaling pathway-related genes through ESCC development, similar to PCN organoids (Figure S8A). A comparative analysis of epithelial cell transcriptomes at each stage in ESCC patient tumors showed increasing similarity as murine ESCC develops under 4-NQO exposure (Figure S8B,C), suggesting that the 4-NQO mouse model recapitulates human ESCC tumorigenesis. Notably, *Ccl2* and *Ccr2* expression in the esophageal epithelial and immune cells, respectively, was the highest in hyperplasia (Figure 5A,B, S8D,E). A further subtype analysis showed that *Ccr2* expression was enriched in the T_{ex} cells and regulatory T (T_{reg}) cells (Figure S8F). Moreover, we found that T_{ex} cell marker (*Cd160*, *Havcr2*/*Tim-3*,

Pdcd1/*Pd-1*, and *Lag3*) expression was increased in the T cells at the early stage of ESCC tumorigenesis (Figure S8G), consistent with our PCN-transplanted tumor cells (Figure 4, S6). To investigate the intercellular CCL-mediated ligand-receptor interaction, epithelial and immune cell communications were analyzed using the Squidpy and CellChat packages. The CCL2-CCR2 interaction was inferred to be strong from the hyperplasia state and maintained until invasive cancer (Figure S8H). Moreover, the total interactions related to the CCL pathway between epithelial cells and immune cells were increased during ESCC development (Figure 5C, S8I). The CCL pathway–specified cell-cell communications were observed starting from the inflammation status in epithelial cells, T_{ex} cells, MDSCs, and macrophages (Figure 5D, S8J).

Given the role of the CCL2-CCR2 axis in the immune evasion of tumor cells,[30] we tested whether the CCL2-CCR2 axis is indispensable for ESCC initiation using two different CCR2 inhibitors (CCR2 22 and BMS-813160). To increase tumorigenic efficiency, we established PCN cells that stably expressed Sox2 (PCNS), as Sox2 promotes ESCC tumorigenicity.[31] Sox2 overexpression accelerated the tumor development of PCN cells while not affecting *Ccl2* expression (Figure S9A-C). Although CCR2 inhibitors did not suppress PCNS cell growth *in vitro*, allograft tumors grown with CCR2 inhibitors were drastically reduced in size and incidence compared to tumors treated with vehicle (Figure 5E, S9D). All tumors exposed to vehicle and CCR2 inhibitors showed abundant immune cell infiltration into the tumors and comparable numbers of proliferating ($Mki67^+$) tumor cells (Figure S9E,F). Consistent with the *Ccl2* KO tumor results, T_{ex} cell ($Pdcd1^+$) infiltration into CCR2-inhibited tumors was markedly decreased, while active $CD8^+$ T cells ($perforin^+$) were enriched in the tumors from CCR2 inhibitor–injected mice compared to in the tumors from vehicle-injected control mice (Figure 5F,G, S9F,G). On the other hand, fewer M2 macrophages were observed in the CCR2-inhibited tumors than in the *Ccl2* KO tumors (Figure 5F,G, S9F). However, the number of other monocyte-derived cells ($CD68^+$ or $CD209^+$) was lower in the CCR2 inhibitor–treated TME, indicating reduced monocyte recruitment by CCR2 blockade (Figure S9F-H). These results suggest that the CCL2-CCR2 axis elicits immune evasion for ESCC initiation.

NF-κB pathway, the upstream regulator of CCL2

Next, we determined the mechanism of CCL2 upregulation during ESCC tumorigenesis. Because CCL2 is upregulated mainly by transcription factors,[32] we sought to identify the key transcription factors that transactivate *CCL2*. An scRNA-seq–based regulon analysis identified PCN-specific regulons (RELA, FOXA1, MYC, TAF1, and TCF12) that may bind to the *Ccl2* promoter (Figure 5H). Among them, Rela was the most highly activated in PCN, and *Ccl2* is expected to be directly transactivated by Rela from a refined analysis using iRegulon (Figure 5I,J). Compared to PN, PCN cells showed more abundant nuclear accumulation of Rela and Rela inhibition downregulated *Ccl2* in PCN cells (Figure 5K,L). Moreover, a chromatin immunoprecipitation (ChIP) assay showed that Rela occupied the *Ccl2* promoter in PCN but not in PN cells, consistent with the results of a previous report that RELA transactivates *CCL2* (Figure 5M).[32, 33] In addition, a human ESCC tissue microarray analysis showed a positive correlation between CCL2 and RELA expression, supporting the pathological relevance of the RELA-CCL2-CCR2 axis to human ESCC tumorigenesis (Figure S9I,J).

Classification of ESCC patients and PCN relevance

To extend our findings to the biology of human ESCC tumorigenesis, we analyzed single-cell transcriptomes of 69 ESCC patient tumor samples (Figure 6A) by integrating human scRNA-seq datasets with the PCN's.[34, 35] The unsupervised principal components analysis and Pearson correlation coefficient categorized 69 patient datasets into three groups (ESC1-3). While ESC1, 2, and 3 constituted a comparable portion of patients (ESC1: 44.9%; ESC2: 29.0%; ESC3: 26.1%) with tumor cell heterogeneity, as described previously,[34] PCN belonged to ESC1 (Figure 6B,C). Notably, ESC1 displayed the lowest pathway score for TP53, CDKN2A, and NOTCH signaling, suggesting that ESC1 has consistent transcriptomic features of PCN EOs (Figure 6B, D). ESC1 and ESC2 showed the highest score for the NF-κB pathway, correlated with *CCL2* expression (Figure 6E,F). Consistent with PCN tumors' immune

landscape, tumor cells of ESC1 patients highly expressed *CD274*/*PD-L1*, suggesting that PCN-type (ESC1) likely has immune escape potential through PD-L1-PD1–mediated T cell exhaustion (Figure 6F, S10A). On the other hand, ESC2 exhibited activation of WNT, PI3K, MAPK, and FGFR1 pathways, whereas ESC3 was enriched with genes related to Hippo, cell cycle, and chromatin modification pathways (Figure S10B,C). Of note, despite the transcriptomic differences among ESC1-3, we could not find categorical differences between the conventional tumor stage classification in the ESC1-3 subtypes (Figure S10D).

We further identified the representative marker genes of each group of patients by DEG analysis. ESC1 showed higher expression of *B2M*, *RGS1*, and *THEMIS2*, which were reported to be highly expressed in several types of cancer.[36-38] *EID1*, *CYB5R3*, and *MGST3* were highly expressed in ESC2, and *MFL2*, *FUS*, and *MDK* were enriched in ESC3 patients (Figure 6G, S10E). Although these markers are upregulated in various cancers,[39-41] they have not been investigated in ESCC. ESCC patients with higher expression of *B2M*, *RGS1*, and *FTL* exhibited poor survival than did those with lower expression (Figure S10F). A TCGA-based analysis also showed that *B2M*, *RGS1*, *MLF2*, *FUS*, and *MDK* were upregulated in ESCC compared to in normal samples (Figure S10G). Immunostaining of the ESCC tissue microarray (n = 101) revealed a positive correlation between B2M and CCL2 expression and B2M and RELA expression (Figure 6H,I, S10H). Most patients (90.9%) had relatively higher B2M expression in tumor samples than in adjacent normal samples, and 22.7% (5 of 22, immunohistochemistry score ≥ 2.5) showed robust expression of both CCL2 and B2M in the tumor tissue (Figure 6J). Focusing on tumor samples alone, 49.0% (25 of 51) of tumor samples expressed high levels of B2M (immunohistochemistry score ≥ 2.5), a similar proportion to ESC1 from scRNA-seq (Figure 6K). These data suggest that B2M is a prognostic marker of ESCC, likely with RELA-CCL2 axis activation.

Discussion

To identify the multiple genetic factors responsible for ESCC initiation, we utilized organoids, which overcome the limitation of single-gene KO (e.g., CRISPR-based screening) and provide a better phenotype analysis (i.e., neoplasia), as further confirmed by a congenic transplantation approach. Inactivation of *Trp53*, *Cdkn2a*, and *Notch1* (PCN) was sufficient to initiate ESCC. While PN and PCN EOs displayed the neoplastic features of ESCC *in vitro*, only PCN cells exhibited *in vivo* tumorigenicity, suggesting immune evasion driven by PCN. A transcriptomic analysis identified that the CCL2-CCR2 axis remodels the immune landscape, confirmed by loss-of-function studies (*Ccl2* KO and CCR2 inhibitors) and a scRNA-seq analysis of the autochthonous mouse model. Finally, using single-cell transcriptomics, we stratified ESCC patients and identified the subtype of PCN-type ESCC patients with new molecular signatures.

Tumor cells evade immune surveillance in various ways.[42, 43] Despite several studies describing the immune landscape of ESCC,[34, 35, 44, 45] experimental demonstrations of ESCC immune evasion have not been achieved. Our comprehensive approaches revealed that *CDKN2A* inactivation plays a crucial role in establishing tumor-favorable niches. Immune profiling of the mouse ESCC model showed decreased effector T cells and increased immune suppressive dendritic cells during ESCC development (Figure 4J,K, S7E,F).[29] Similarly, human ESCC generates an immune-suppressive landscape with enriched T_{ex} or T_{reg} cells and upregulation of immunosuppression-related genes in TAMs and dendritic cells.[34, 35, 46] Notably, enriched T_{ex} cells and TAMs are commonly observed in mouse scRNA-seq–based immune profiling and PCN TME (Figure 4J,K, S7E,F), unveiling the distinct immune niche of PCN-associated ESCC tumorigenesis.

We found that CCL2 is the key immune landscape remodeling factor for ESCC initiation, mainly represented by increased T_{ex} cells and M2-like macrophages and a reduced number of effector $CD8^+$ T and dendritic cells. The CCL2-CCR2 axis induces

tumor-favorable TME.[47] Given the high expression of CCR2 in monocytes, CCR2-mediated M2-like macrophage differentiation and polarization has been studied in the context of tumor cell invasion and metastasis.[27] Additionally, the CCL2-CCR2 axis was shown to induce TAM accumulation.[30] Moreover, CCR2 expressed in T cells modulates the recruitment of T_{reg} cells,[48] hampering immune surveillance. Therefore, targeting the CCL2-CCR2 axis to enhance immune surveillance may be a promising option for ESCC treatment. Indeed, blocking the CCL2-CCR2 axis has been tested in clinical trials in other types of cancer, with ICIs.[28, 47, 49] However, since CCL2 is a chemoattractant that recruits monocytes, systemic inhibition of the CCL2-CCR2 axis might affect normal immune surveillance. For instance, impaired monocyte recruitment by CCR2 blockade could reduce the number of antigen-presenting cells, diminishing innate and adaptive immune responses critical for anti-cancer effects.[50] Our results showed that the transient inhibition of CCR2 suppressed tumor growth, but monocyte-derived cell ($CD209^+$ or $CD68^+$) recruitment was decreased. In contrast, the number of $CD8^+$ T cells was not significantly increased compared to the TME of *Ccl2* KO tumors (Figure 5, S9). Therefore, targeting CCL2 or the upstream molecules of CCL2 in tumor cells would minimize potential adverse effects.

Recent clinical trials showed promising outcomes of ICIs in patients with advanced ESCC.[10-14] Nonetheless, ESCC patient stratification is a significant hurdle. Although the datasets from the 69 patients analyzed in this study lacked ICI-related clinical information, PCN-type (ESC1) patients showed higher expression of *PD-L1*/*CD274* than did other patients. Thus, CCL2-CCR2 blockade combined with PD-L1 or PD-1 ICIs could be effective in ESC1 patients, and B2M could be a signature for ESC1 subtype (Figure 6G, S10E), potentially allowing a molecular signature-guided ICI strategy.

Together, this study identifies the inactivation of *TP53*, *CDKN2A*, and *NOTCH1* as important genetic events leading to ESCC development, accompanied by immune evasion, and newly classifies ESCC patients based on the molecular features of tumor cell transcriptomes.

476

References

1. Pennathur A, Gibson MK, Jobe BA, et al. Oesophageal carcinoma. The Lancet 2013;381:400-412.
2. Wang GQ, Abnet CC, Shen Q, et al. Histological precursors of oesophageal squamous cell carcinoma: results from a 13 year prospective follow up study in a high risk population. Gut 2005;54:187-92.
3. Board PATE. Esophageal Cancer Treatment (Adult) (PDQ(R)): Patient Version. PDQ Cancer Information Summaries. Bethesda (MD), 2002.
4. **Bejarano L, Jordao MJC**, Joyce JA. Therapeutic Targeting of the Tumor Microenvironment. Cancer Discov 2021;11:933-959.
5. Hinshaw DC, Shevde LA. The Tumor Microenvironment Innately Modulates Cancer Progression. Cancer Res 2019;79:4557-4566.
6. **Keskin DB, Anandappa AJ, Sun J**, et al. Neoantigen vaccine generates intratumoral T cell responses in phase Ib glioblastoma trial. Nature 2019;565:234-239.
7. Friedl P, Alexander S. Cancer invasion and the microenvironment: plasticity and reciprocity. Cell 2011;147:992-1009.
8. Baba Y, Nomoto D, Okadome K, et al. Tumor immune microenvironment and immune checkpoint inhibitors in esophageal squamous cell carcinoma. Cancer Sci 2020;111:3132-3141.
9. Luan S, Zeng X, Zhang C, et al. Advances in Drug Resistance of Esophageal Cancer: From the Perspective of Tumor Microenvironment. Front Cell Dev Biol 2021;9:664816.
10. Wang ZX, Cui C, Yao J, et al. Toripalimab plus chemotherapy in treatment-naive, advanced esophageal squamous cell carcinoma (JUPITER-06): A multi-center phase 3 trial. Cancer Cell 2022;40:277-288 e3.
11. Sun JM, Shen L, Shah MA, et al. Pembrolizumab plus chemotherapy versus chemotherapy alone for first-line treatment of advanced oesophageal cancer (KEYNOTE-590): a randomised, placebo-controlled, phase 3 study. Lancet 2021;398:759-771.
12. Doki Y, Ajani JA, Kato K, et al. Nivolumab Combination Therapy in Advanced Esophageal Squamous-Cell Carcinoma. N Engl J Med 2022;386:449-462.
13. Yamamoto S, Kato K. JUPITER-06 establishes immune checkpoint inhibitors as essential first-line drugs for the treatment of advanced esophageal squamous cell carcinoma. Cancer Cell 2022;40:238-240.
14. Okada M, Kato K, Cho BC, et al. Three-Year Follow-Up and Response-Survival Relationship of Nivolumab in Previously Treated Patients with Advanced Esophageal Squamous Cell Carcinoma (ATTRACTION-3). Clin Cancer Research 2022;28.

15. Miyoshi H, Stappenbeck TS. In vitro expansion and genetic modification of gastrointestinal stem cells in spheroid culture. Nat Protoc 2013;8:2471-2482.

16. Ko KP, Zhang J, Park JI. Establishing transgenic murine esophageal organoids. STAR Protoc 2022;3:101317.

17. Gao YB, Chen ZL, Li JG, et al. Genetic landscape of esophageal squamous cell carcinoma. Nat Genet 2014;46:1097-1102.

18. Song Y, Li L, Ou Y, et al. Identification of genomic alterations in oesophageal squamous cell cancer. Nature 2014;509:91-95.

19. **Zheng B, Ko KP**, Fang X, et al. A new murine esophageal organoid culture method and organoid-based model of esophageal squamous cell neoplasia. iScience 2021;24:103440.

20. Tang Q, Efe G, Chiarella AM, et al. Mutant p53 regulates Survivin to foster lung metastasis. Genes Dev 2021;35:528-541.

21. Board PATE. Esophageal Cancer Treatment (PDQ(R)): Health Professional Version. PDQ Cancer Information Summaries. Bethesda (MD), 2002.

22. Okawa T, Michaylira CZ, Kalabis J, et al. The functional interplay between EGFR overexpression, hTERT activation, and p53 mutation in esophageal epithelial cells with activation of stromal fibroblasts induces tumor development, invasion, and differentiation. Genes Dev 2007;21:2788-803.

23. Busslinger GA, Weusten BLA, Bogte A, et al. Human gastrointestinal epithelia of the esophagus, stomach, and duodenum resolved at single-cell resolution. Cell Rep 2021;34:108819.

24. **Kinker GS, Greenwald AC**, Tal R, et al. Pan-cancer single-cell RNA-seq identifies recurring programs of cellular heterogeneity. Nat Genet 2020;52:1208-1218.

25. Popivanova BK, Kostadinova FI, Furuichi K, et al. Blockade of a chemokine, CCL2, reduces chronic colitis-associated carcinogenesis in mice. Cancer Res 2009;69:7884-7892.

26. Hao Q, Vadgama JV, Wang P. CCL2/CCR2 signaling in cancer pathogenesis. Cell Commun Signal 2020;18:82.

27. Qian BZ, Li J, Zhang H, et al. CCL2 recruits inflammatory monocytes to facilitate breast-tumour metastasis. Nature 2011;475:222-225.

28. Tu MM, Abdel-Hafiz HA, Jones RT, et al. Inhibition of the CCL2 receptor, CCR2, enhances tumor response to immune checkpoint therapy. Commun Biol 2020;3:720.

29. **Yao J, Cui Q, Fan W**, et al. Single-cell transcriptomic analysis in a mouse model deciphers cell transition states in the multistep development of esophageal cancer. Nature Communications 2020;11.

30. Yang H, Zhang Q, Xu M, et al. CCL2-CCR2 axis recruits tumor associated macrophages to induce immune evasion through PD-1 signaling in esophageal carcinogenesis. Mol Cancer 2020;19:41.

31. **Wu Z, Zhou J, Zhang X**, et al. Reprogramming of the esophageal squamous carcinoma epigenome by SOX2 promotes ADAR1 dependence. Nat Genet 2021;53:881-894.

32. Jin J, Lin J, Xu A, et al. CCL2: An Important Mediator Between Tumor Cells and Host Cells in Tumor Microenvironment. Front Oncol 2021;11:722916.

33. Ueda A, Okuda K, Ohno S, et al. NF-kappa B and Sp1 regulate transcription of the human monocyte chemoattractant protein-1 gene. J Immunol 1994;153:2052-2063.

34. **Zhang X, Peng L, Luo Y**, et al. Dissecting esophageal squamous-cell carcinoma ecosystem by single-cell transcriptomic analysis. Nat Commun 2021;12:5291.

35. **Dinh HQ, Pan F, Wang G**, et al. Integrated single-cell transcriptome analysis reveals heterogeneity of esophageal squamous cell carcinoma microenvironment. Nat Commun 2021;12:7335.

36. **Zhang H, Cui B**, Zhou Y, et al. B2M overexpression correlates with malignancy and immune signatures in human gliomas. Sci Rep 2021;11:5045.

37. Li SL, Yang HX, Li SL, et al. High expression of regulator of G-protein signalling 1 is associated with the poor differentiation and prognosis of gastric cancer. Oncology Letters 2021;21.

38. Wu T, Li Y, Liu B, et al. Expression of Ferritin Light Chain (FTL) Is Elevated in Glioblastoma, and FTL Silencing Inhibits Glioblastoma Cell Proliferation via the GADD45/JNK Pathway. PLoS One 2016;11:e0149361.

39. Miyake S, Sellers WR, Safran M, et al. Cells degrade a novel inhibitor of differentiation with E1A-like properties upon exiting the cell cycle. Molecular and Cellular Biology 2000;20:8889-8902.

40. Lund RR, Leth-Larsen R, Caterino TD, et al. NADH-Cytochrome b5 Reductase 3 Promotes Colonization and Metastasis Formation and Is a Prognostic Marker of Disease-Free and Overall Survival in Estrogen Receptor-Negative Breast Cancer. Mol Cell Proteomics 2015;14:2988-2999.

41. Filippou PS, Karagiannis GS, Constantinidou A. Midkine (MDK) growth factor: a key player in cancer progression and a promising therapeutic target. Oncogene 2020;39:2040-2054.

42. Spranger S, Gajewski TF. Impact of oncogenic pathways on evasion of antitumour immune responses. Nat Rev Cancer 2018;18:139-147.

43. Togashi Y, Shitara K, Nishikawa H. Regulatory T cells in cancer immunosuppression - implications for anticancer therapy. Nat Rev Clin Oncol 2019;16:356-371.

44. Chen Z, Zhao M, Liang J, et al. Dissecting the single-cell transcriptome network underlying esophagus non-malignant tissues and esophageal squamous cell carcinoma. EBioMedicine 2021;69:103459.

45. Stairs DB, Bayne LJ, Rhoades B, et al. Deletion of p120-catenin results in a tumor microenvironment with inflammation and cancer that establishes it as a tumor suppressor gene. Cancer Cell 2011;19:470-83.

46. Zheng Y, Chen Z, Han Y, et al. Immune suppressive landscape in the human esophageal squamous cell carcinoma microenvironment. Nat Commun 2020;11:6268.

47. Fei L, Ren X, Yu H, et al. Targeting the CCL2/CCR2 Axis in Cancer Immunotherapy: One Stone, Three Birds? Front Immunol 2021;12:771210.

48. Loyher PL, Rochefort J, Baudesson de Chanville C, et al. CCR2 Influences T Regulatory Cell Migration to Tumors and Serves as a Biomarker of Cyclophosphamide Sensitivity. Cancer Res 2016;76:6483-6494.

49. Flores-Toro JA, Luo D, Gopinath A, et al. CCR2 inhibition reduces tumor myeloid cells and unmasks a checkpoint inhibitor effect to slow progression of resistant murine gliomas. Proc Natl Acad Sci U S A 2020;117:1129-1138.

50. Peters W, Dupuis M, Charo IF. A mechanism for the impaired IFN-gamma production in C-C chemokine receptor 2 (CCR2) knockout mice: role of CCR2 in linking the innate and adaptive immune responses. J Immunol 2000;165:7072-7077.

Author names in bold designate shared co-first authorship.

Figure Legends

Figure 1. Genetic ablation of *Trp53* and *Notch1* induces esophageal hyperplasia and de-differentiation.

A, Schematic structure of murine EOs.

B, Heatmap visualizing the volume of each EO.

C, Hematoxylin-and-eosin (H&E) images; scale bars = 50 μm.

D,E, Immunofluorescent (IF) images of EOs (D); MKI67+ cell quantification (E). WT: *Trp53*$^{floxed/floxed}$, N: *Notch1* KO, C: *Cdkn2a* KO, CN: *Cdkn2a* KO + *Notch1* KO, P: *Trp53*$^{del/del}$, PN: *Trp53*$^{del/del}$ + *Notch1* KO, PC: *Trp53*$^{del/del}$ + *Cdkn2a* KO, PCN: *Trp53*$^{del/del}$ + *Cdkn2a* KO + *Notch1* KO; scale bars = 20 μm; ****$P < 0.0001$.

F, IF staining images; scale bars = 20 μm.

G,H, BrdU incorporation assays; IF with anti-BrdU antibody (G); BrdU+ cell quantification (H); scale bars = 10 μm; ****$P < 0.0001$.

I,J, Bright-field images of EOs co-cultured with mesenchymal (Tomato [red] fluorescent-expressing) cells (I); E-cadherin/CDH1 IF images of EOs (J); scale bars = 50 μm.

K,L, Assessing colony formation ability (K) and cell growth rate (L) of EOs.

Figure 2. **Single-cell transcriptomic analysis of genetically engineered EOs.**

A, Schematic overview of scRNA-seq procedure. Four types of EOs (WT, PC, PN, and PCN) were multiplexed for library preparation.

B,C, UMAPs of four integrated datasets.

D, The proportion of each cluster was compared to the same cluster of the WT dataset. Statistical significance between 2 groups was assessed by the permutation test.

E, RNA velocity–based UMAP projection based on cell types in each dataset.

F, Cell trajectory inference by RNA velocity.

G, Latent time results projected on the velocity-based UMAP.

H, PAGA analysis of RNA velocity–based cell clusters showing the direction of cell lineage on UMAP. The size of the circle corresponds to the cell number.

I, Representative marker genes of root cell clusters with simplified lineage trajectories.

Figure 3. Transcriptomes of PN and PCN recapitulate the ESCC phenotype.

A, Dot plot of ESCC stem cell markers.

B,C, ESCC phenotype–associated cells were marked as $ESCC^+$ cells in Scissor-based UMAP projection (B), and the proportion of $ESCC^+$ cells is shown in bar plot (C). ****P value < 0.0001, as determined by Fisher's exact test.

D,E, Poor survival of ESCC patient–associated cells is displayed as Poor $survival^+$ cells in UMAP (D), and the proportion was analyzed (E). ****P value < 0.0001, as determined by Fisher's exact test. n.s. = not significant.

F, Gene set enrichment analysis of PN or PCN dataset.

G, Heatmap clustering of bulk RNA-sequencing from WT, PN, and PCN EOs.

H, Enrichr from bulk RNA-seq datasets. PN- or PCN-enriched genes compared to WT were analyzed using Bioplanet and REACTOME databases; TOP5 features of each database are shown; *P value.

I, Dot plots of PN or PCN highly expressed genes compared to gene sets of the Kyoto Encyclopedia of Genes and Genomes (KEGG) pathways; dot size: gene number count; dot colors: adjusted P values.

Figure 4. *In vivo* tumorigenicity of PCN with pro-tumorigenic TME.

A, Assessment of tumor growth from C57BL/6 mice subcutaneously injected with either PN or PCN cells.

B, H&E images; red arrowheads, mitotic cells; black arrowhead, blood vessel; dotted circle, inflammatory cells; scale bars = 100 μm.

C, IF images of transplanted tumors; scale bars = 100 μm.

D, Enrichr analysis from DEGs of PCN and PN scRNA-seq datasets.

E, Volcano plot of DEGs between PCN and PN datasets.

F, Feature plot of *Ccl2*.

G-I, Tumor assessment of mice subcutaneously transplanted with PCN or PCN-*Ccl2* KO cells; tumor images (G), tumor volume (H), and weight (I) comparison.

J, PDCD1$^+$, PRF1/PERFORIN$^+$, CD8$^+$, CD206$^+$, CD209$^+$, and MKI67$^+$ cells in randomly chosen 630× magnified images were analyzed and plotted. n.s. = not significant.

K, PDCD1/PD-1, PRF1/PERFORIN, CD8, CD206, CD209, and MKI67 staining of PCN and PCN-*Ccl2* KO–derived tumors. Scale bars = 20 μm.

Figure 5. CCL2-CCR2-induced immune evasion during ESCC development.

A, Dot plot visualizing epithelial cells' *Ccl2* expression of each disease status.

B, Dot plot showing *Ccr2* expression in immune cells based on the disease status.

C, Circle plots visualizing ligand-receptor interactions related to CCL pathway in sub-clusters of immune and epithelial cells using 'CellChat' package.

D, Chord diagrams displaying significant interactions of the CCL pathway in epithelial cells with T_{ex} cell, MDSC, and macrophage sub-clusters. Directions from ligands (epithelial cell) to receptors (immune cell) are indicated.

E, Tumors from Sox2-overexpressed PCN (PCNS) cell–transplanted mice were monitored and measured after intraperitoneal injection (days 17, 21, and 25) of Ccr2 inhibitors (CCR2 22 and BMS-813160) or DMSO (vehicle control); ***P < 0.001, ****P < 0.0001.

F,G, Microscopic analyses of vehicle-, CCR2 22-, and BMS-813160-treated tumors; quantification (F) of IF images (G); scale bars = 20 μm, *P < 0.05, **P < 0.01, ***P < 0.001, ****P < 0.0001.

H, Venn diagram showing overlapped transcription factors of the UCSC ChIP seq database and PN- and PCN-specific regulons.

I, Rela regulon projection in regulon-based UMAP of WT, PC, and PCN datasets. The color shows regulon specificity score of the cells.

J, Network analysis of transcription factors related to human Ccl2 gene expression. Target genes of transcription factors were refined by iRegulon, and the Ccl2 connections to Taf1 and Rela are displayed.

K, Rela immunofluorescence images of 2D-cultured PN and PCN. Nuclei were stained with DAPI. Scale bar = 10 μm. The proportion of cells with nuclear-accumulated Rela was evaluated in PN and PCN cells.

L, qRT-PCR results showing Ccl2 expression in PCN cells treated with different doses of NF-κB inhibitor for 6 hrs.

M, ChIP assays showing binding activity of Rela to Ccl2 promoter in PN and PCN cells. Putative Rela binding sites (a, b, and c) and non-binding sites in the distant region (d) were analyzed with eluted DNA fragment amplification by PCR.

Figure 6. **Classification of ESCC patients and PCN relevance.**

A, Integrated UMAP of tumor epithelial cells of 69 ESCC patients and PCN organoids.

B, Correlation matrix heatmap of integrated datasets of ESCC patients and PCN organoids. The dendrogram showing the distance of each dataset based on principal component analysis with the Pearson correlation (a color spectrum) and pathway scores (TP53, CDKN2A, and NOTCH). PCN was excluded for pathway scores.

C, UMAP showing ESCC subtypes.

D-F, Dot plots of pathway scores (TP53, CDKN2A, and NOTCH) (D), NF-κB score (E), and *CCL2*, *CD274*/*PD-L1*, and *PDCD1LG2*/*PD-L2* gene expression (F) in ESCC subtypes.

G, Dot plot of ESCC subtype's representative marker genes selected from DEG analysis using the Wilcoxon method.

H,I, B2M and CCL2 staining of human ESCC tissue microarray samples (**H**) and the correlation of the results (I); scale bars = 50 μm (upper) and 20 μm (lower); r: Pearson correlation coefficient; *P*: *P* values; N: number of samples.

J,K, Heatmap of B2M staining results in tumor samples (J) and B2M, CCL2, and RELA staining results in ESCC patients with adjacent normal and tumor paired samples (K). Immunohistochemistry scores displayed from 1 (lowest) to 3 (highest) expression.

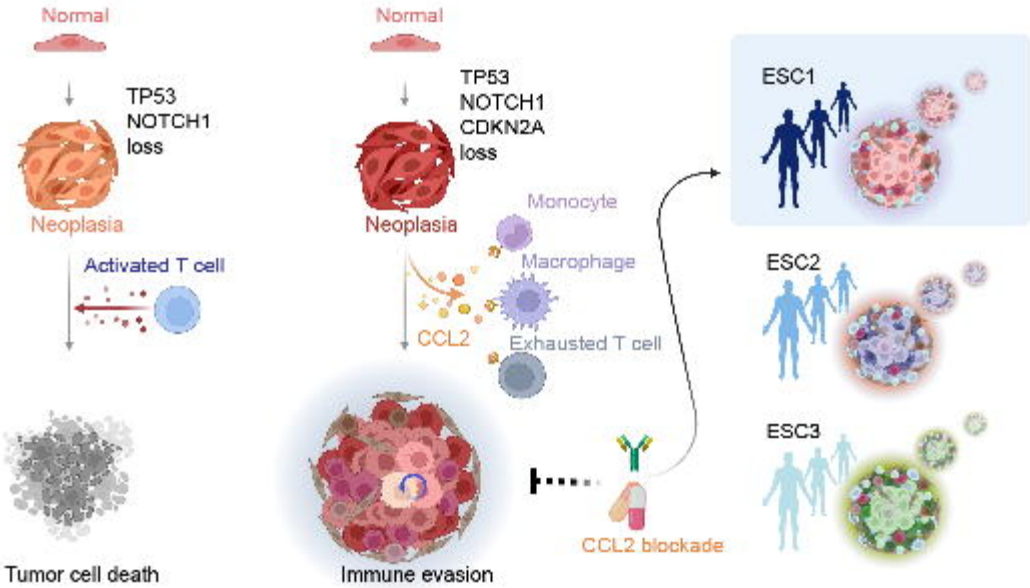
Normal
TP53
NOTCH1
loss
Neoplasia
Activated T cell
Tumor cell death
Normal
TP53
NOTCH1
CDKN2A
loss
Neoplasia
Monocyte
Macrophage
CCL2
Exhausted T cell
Immune evasion
CCL2 blockade
ESC1
ESC2
ESC3

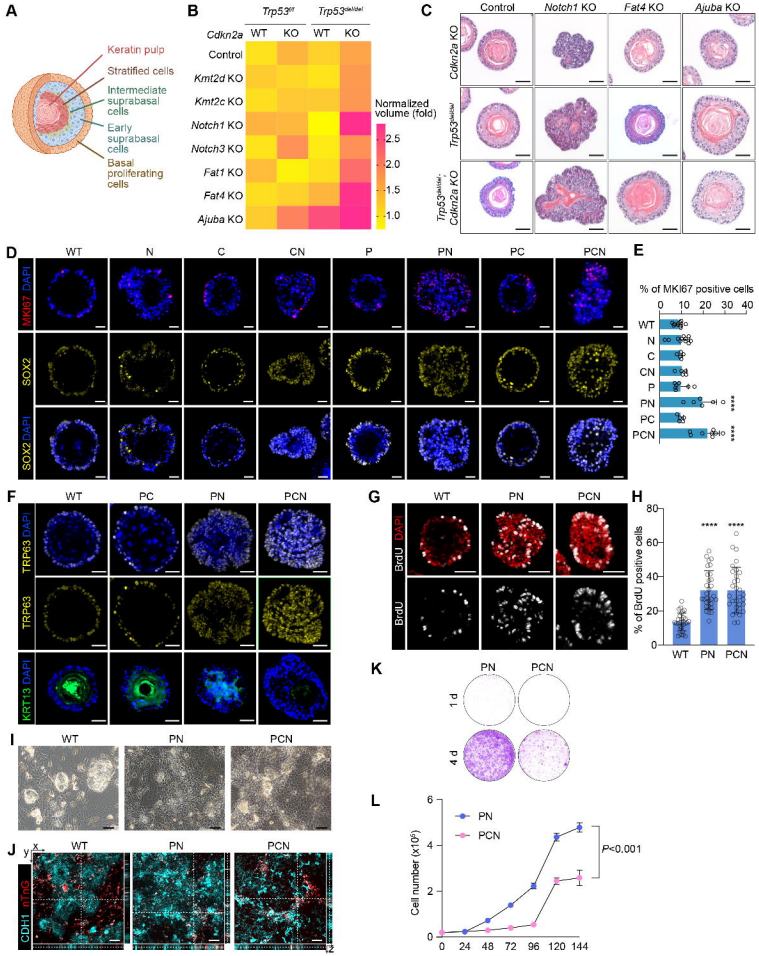
A
Keratin pulp
Stratified cells
Intermediate suprabasal cells
Early suprabasal cells
Basal proliferating cells
B
Trp53f/f
Trp53del/del
WT
KO
WT
KO
Cdkn2a
Control
Kmt2d KO
Kmt2c KO
Notch1 KO
Notch3 KO
Fat1 KO
Fat4 KO
Ajuba KO
Normalized volume (fold)
2.5
2.0
1.5
1.0
C
Control
Notch1 KO
Fat4 KO
Ajuba KO
Cdkn2a KO
Trp53del/del
Trp53del/del; Cdkn2a KO
D
WT
N
C
CN
P
PN
PC
PCN
MKI67 DAPI
SOX2
SOX2 DAPI
E
% of MKI67 positive cells
0
10
20
30
40
WT
N
C
CN
P
PN
PC
PCN
****
****
F
WT
PC
PN
PCN
TRP63 DAPI
TRP63
KRT13 DAPI
G
WT
PN
PCN
BrdU DAPI
BrdU
H
% of BrdU positive cells
80
60
40
20
0
****
****
WT
PN
PCN
I
WT
PN
PCN
J
y
x
WT
PN
PCN
CDH1 nTdG
K
PN
PCN
1 d
4 d
L
PN
PCN
Cell number (x10⁵)
6
4
2
0
P<0.001
0
24
48
72
96
120
144
Time (h)

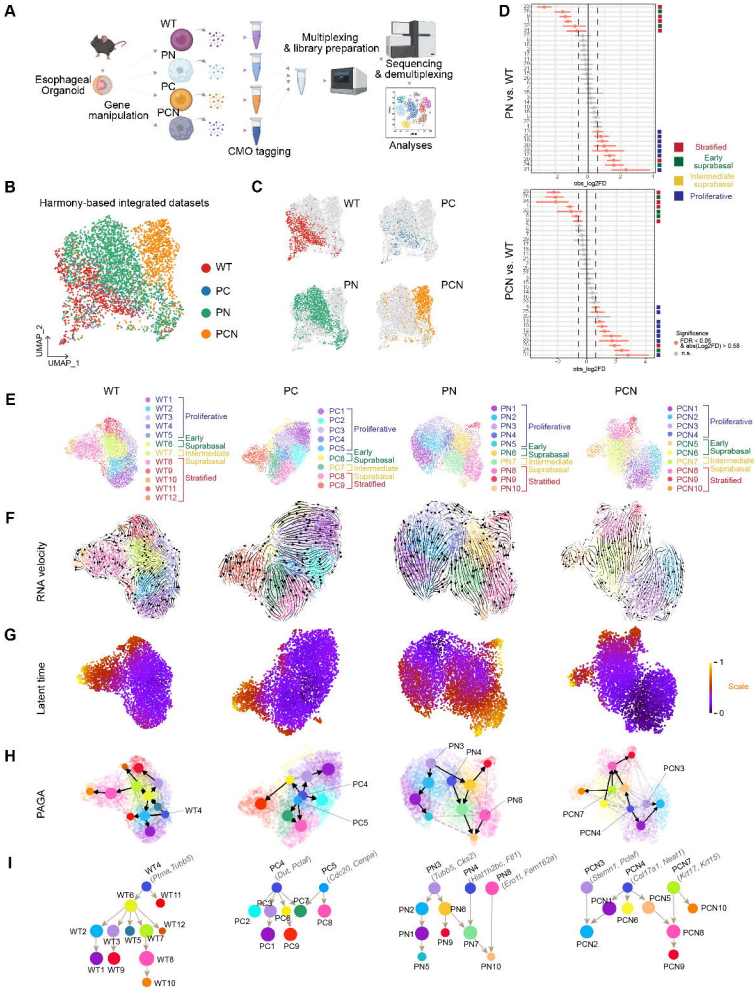
A
WT
PN
PC
PCN
Esophageal Organoid
Gene manipulation
CMO tagging
Multiplexing & library preparation
Sequencing & demultiplexing
Analyses
B
Harmony-based integrated datasets
WT
PC
PN
PCN
UMAP_2
UMAP_1
C
WT
PC
PN
PCN
D
PN vs. WT
PCN vs. WT
obs_log2FD
Stratified
Early suprabasal
Intermediate suprabasal
Proliferative
Significance
FDR < 0.05
& abs(Log2FD) > 0.58
n.s.
E
WT
PC
PN
PCN
Proliferative
Early Suprabasal
Intermediate Suprabasal
Stratified
F
RNA velocity
G
Latent time
Scale
H
PAGA
I
WT4 (Ptma, Tubb5)
PC4 (Dut, Pclaf)
PC5 (Cdc20, Cenpa)
PN3 (Tubb5, Cks2)
PN4 (Hist1h2bc, Ftl1)
PN8 (Ero1l, Fem1b2a)
PCN3 (Stemn1, Pclaf)
PCN4 (Cdr17a1, Neat1)
PCN7 (Krt17, Krt15)

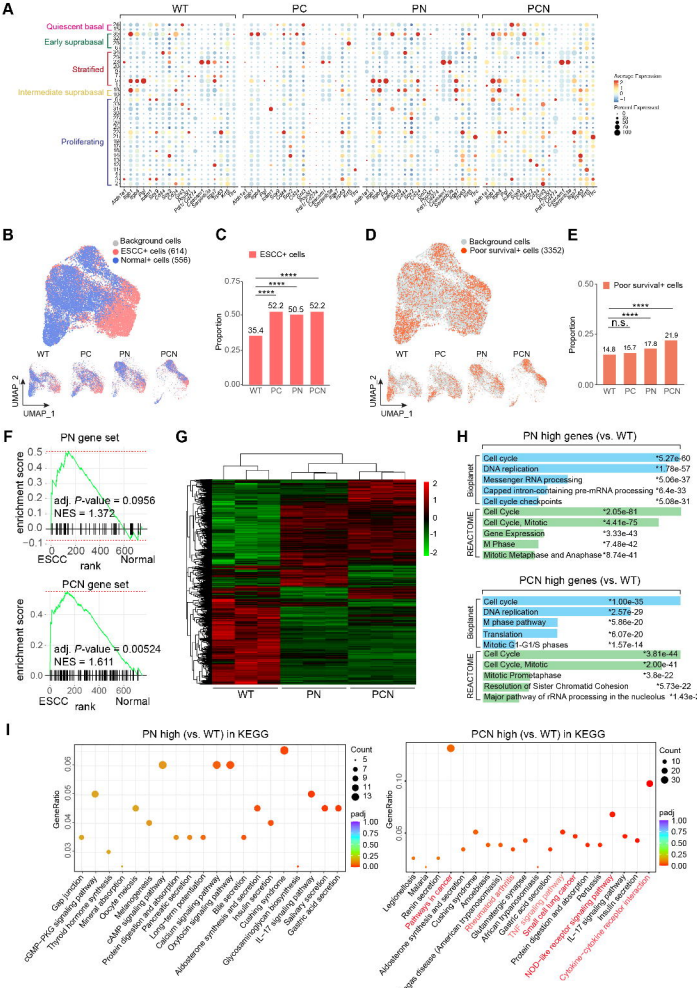
A
WT
PC
PN
PCN
Quiescent basal
Early suprabasal
Stratified
Intermediate suprabasal
Proliferating
Average Expression
Percent Expressed
B
Background cells
ESCC+ cells (614)
Normal+ cells (556)
UMAP_2
UMAP_1
C
ESCC+ cells
Proportion
35.4
52.2
50.5
52.2
D
Background cells
Poor survival+ cells (3352)
E
Poor survival+ cells
n.s.
14.8
15.7
17.8
21.9
F
PN gene set
enrichment score
adj. P-value = 0.0956
NES = 1.372
ESCC
Normal
rank
PCN gene set
adj. P-value = 0.00524
NES = 1.611
G
H
PN high genes (vs. WT)
Bioplanet
Cell cycle *5.27e-60
DNA replication *1.78e-57
Messenger RNA processing *5.06e-37
Capped intron-containing pre-mRNA processing *6.4e-33
Cell cycle checkpoints *5.08e-31
REACTOME
Cell Cycle *2.05e-81
Cell Cycle, Mitotic *4.41e-75
Gene Expression *3.33e-43
M Phase *7.48e-42
Mitotic Metaphase and Anaphase *8.74e-41
PCN high genes (vs. WT)
Cell cycle *1.00e-35
DNA replication *2.57e-29
M phase pathway *5.86e-20
Translation *6.07e-20
Mitotic G1-G1/S phases *1.57e-14
Cell Cycle *3.81e-44
Cell Cycle, Mitotic *2.00e-41
Mitotic Prometaphase *3.8e-22
Resolution of Sister Chromatid Cohesion *5.73e-22
Major pathway of rRNA processing in the nucleolus *1.43e-20
I
PN high (vs. WT) in KEGG
GeneRatio
Count
padj
Gap junction
cGMP-PKG signaling pathway
Thyroid hormone synthesis
Mineral absorption
Oxyte rebasis
Melanogenesis
cAMP signaling pathway
Protein digestion and absorption
Pancreatic secretion
Long-term potentiation
Calcium signaling pathway
Oxytocin signaling pathway
Aldosterone synthesis and secretion
Insulin secretion
Cushing syndrome
Glycosaminoglycan biosynthesis
IL-17 signaling pathway
Salivary secretion
Gastric acid secretion
PCN high (vs. WT) in KEGG
Legionellosis
Malaria
Parietal secretion
Pathways in cancer
Aldosterone synthesis and secretion
Cushing syndrome
Amoebiasis
Chagas disease (American trypanosomiasis)
Rheumatoid arthritis
Glutamatergic synapse
African trypanosomiasis
Gastric acid secretion
Thyroid signaling pathway
Small cell lung cancer
Protein digestion and absorption
Insulin secretion
NOD-like receptor signaling pathway
IL-17 signaling pathway
Cytokine-cytokine receptor interaction

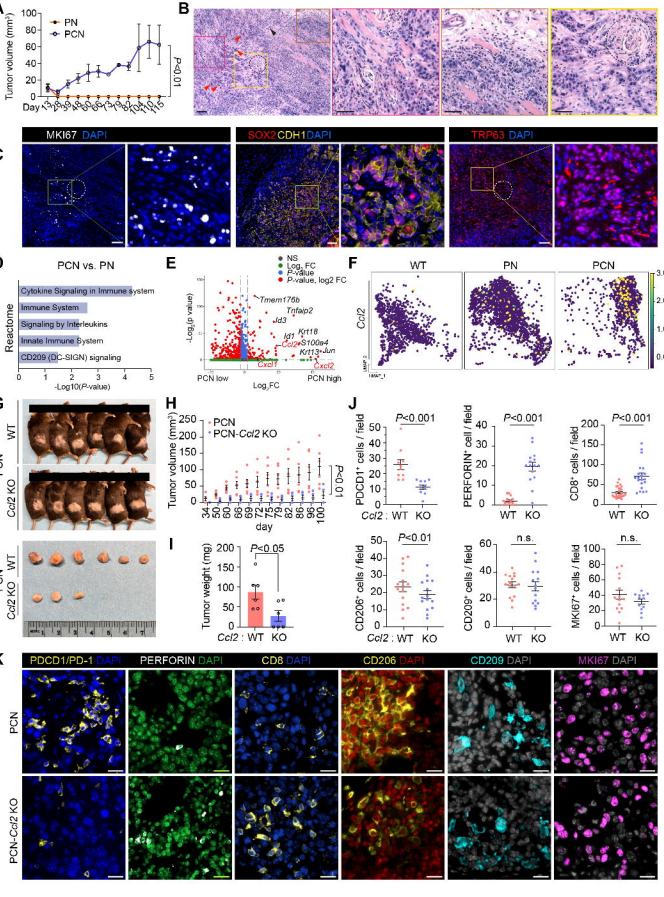

A
Tumor volume (mm³)
PN
PCN
P<0.01
Day
B
C
MKI67 DAPI
SOX2 CDH1 DAPI
TRP63 DAPI
D
PCN vs. PN
Reactome
Cytokine Signaling in Immune system
Immune System
Signaling by Interleukins
Innate Immune System
CD209 (DC-SIGN) signaling
-Log10(P-value)
E
NS
Log2 FC
P-value
P-value, log2 FC
Tmem176b
Tnfalp2
Id3
Id1
Kyt18
Ccl2
S100a4
Kit13
Jun
Cxcl1
Cxcl2
-Log10(p value)
PCN low
PCN high
Log2FC
F
WT
PN
PCN
Ccl2
G
WT
PCN
Ccl2 KO
H
PCN
PCN-Ccl2 KO
Tumor volume (mm³)
P<0.01
day
I
Tumor weight (mg)
P<0.05
Ccl2 : WT KO
J
P<0.001
PDCD1+ cells / field
PERFORIN+ cell / field
CD8+ cells / field
P<0.01
CD206+ cells / field
CD209+ cells / field
n.s.
MKI67+ cells / field
K
PDCD1/PD-1 DAPI
PERFORIN DAPI
CD8 DAPI
CD206 DAPI
CD209 DAPI
MKI67 DAPI
PCN
PCN-Ccl2 KO

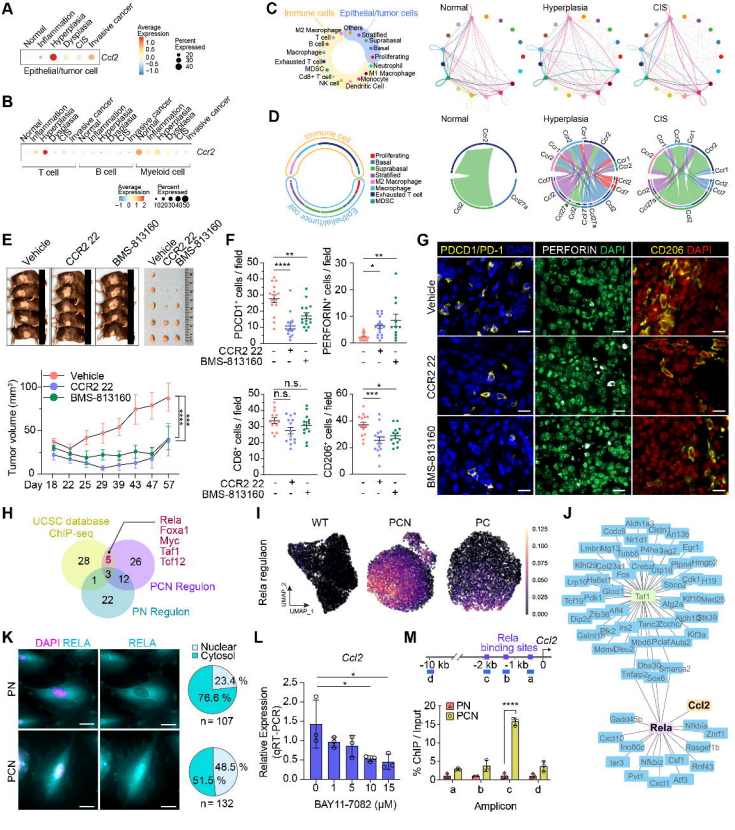
A
Normal
Inflammation
Hyperplasia
CIS
Invasive cancer
Ccl2
Epithelial/tumor cell
Average Expression
Percent Expressed
B
Ccr2
T cell
B cell
Myeloid cell
C
Immune cells
Epithelial/tumor cells
Normal
Hyperplasia
CIS
D
Immune cell
Epithelial/tumor cell
Proliferating
Basal
Suprabasal
Stratified
M2 Macrophage
Macrophage
Exhausted T cell
MDSC
E
Vehicle
CCR2 22
BMS-813160
Tumor volume (mm³)
Day 16 22 25 29 39 43 47 57
F
PDCD1+ cells / field
PERFORIN+ cells / field
CD8+ cells / field
CD206+ cells / field
G
PDCD1/PD-1 DAPI
PERFORIN DAPI
CD206 DAPI
H
UCSC database
ChIP-seq
Rela
Foxa1
Myc
Taf1
Tcf12
PCN Regulon
PN Regulon
I
WT
PCN
PC
Rela regulaon
UMAP_1
UMAP_2
J
Ccl2
Rela
K
DAPI RELA
RELA
PN
PCN
Nuclear
Cytosol
23.4 %
76.6 %
n= 107
48.5 %
51.5 %
n= 132
L
Ccl2
Relative Expression (qRT-PCR)
BAY11-7082 (μM)
M
Rela binding sites
Ccl2
% ChIP / Input
PN
PCN
Amplicon

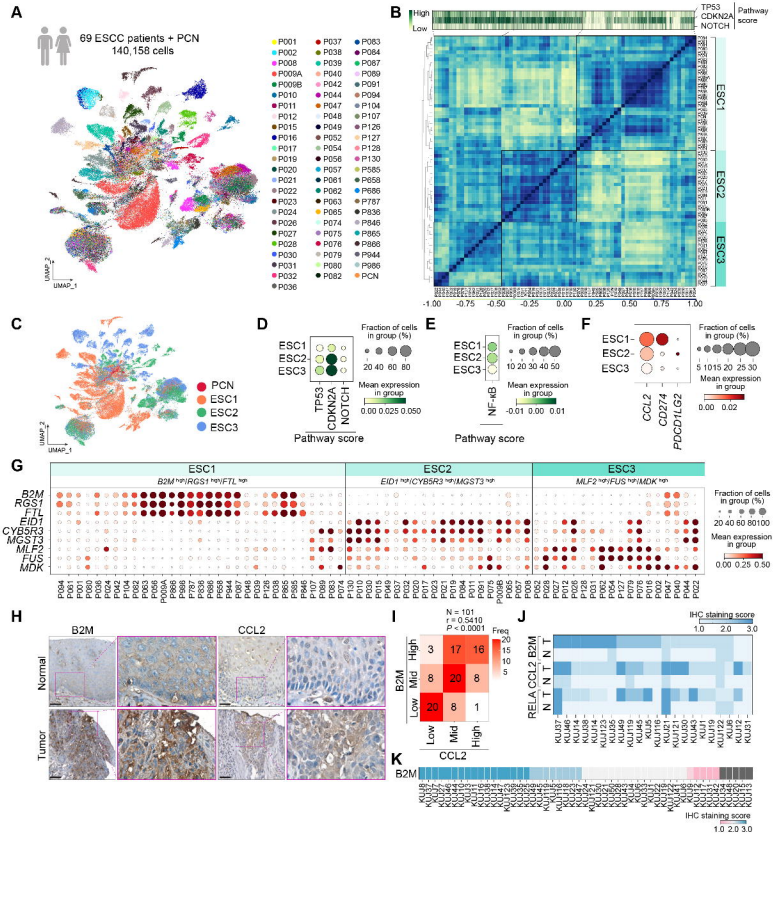
A
69 ESCC patients + PCN
140,158 cells
UMAP_1
UMAP_2
B
High
Low
TP53
CDKN2A
NOTCH
Pathway score
ESC1
ESC2
ESC3
-1.00 -0.75 -0.50 -0.25 0.00 0.25 0.50 0.75 1.00
C
PCN
ESC1
ESC2
ESC3
D
Fraction of cells in group (%)
20 40 60 80
Mean expression in group
0.00 0.025 0.050
Pathway score
E
NF-κB
10 20 30 40 50
-0.01 0.00 0.01
F
CCL2
CD274
PDCD1LG2
5 10 15 20 25 30
0.00 0.02
G
ESC1
B2M hi/RGS1 hi/FTL hi
ESC2
EID1 hi/CYB5R3 hi/MGST3 hi
ESC3
MLF2 hi/FUS hi/MDK hi
B2M
RGS1
FTL
EID1
CYB5R3
MGST3
MLF2
FUS
MDK
0.00 0.25 0.50
H
B2M
CCL2
Normal
Tumor
I
N = 101
r = 0.5410
P < 0.0001
Freq
B2M
CCL2
High
Mid
Low
3 17 16
8 20 8
20 8 1
J
IHC staining score
1.0 2.0 3.0
B2M
CCL2
RELA
K
B2M
IHC staining score
1.0 2.0 3.0

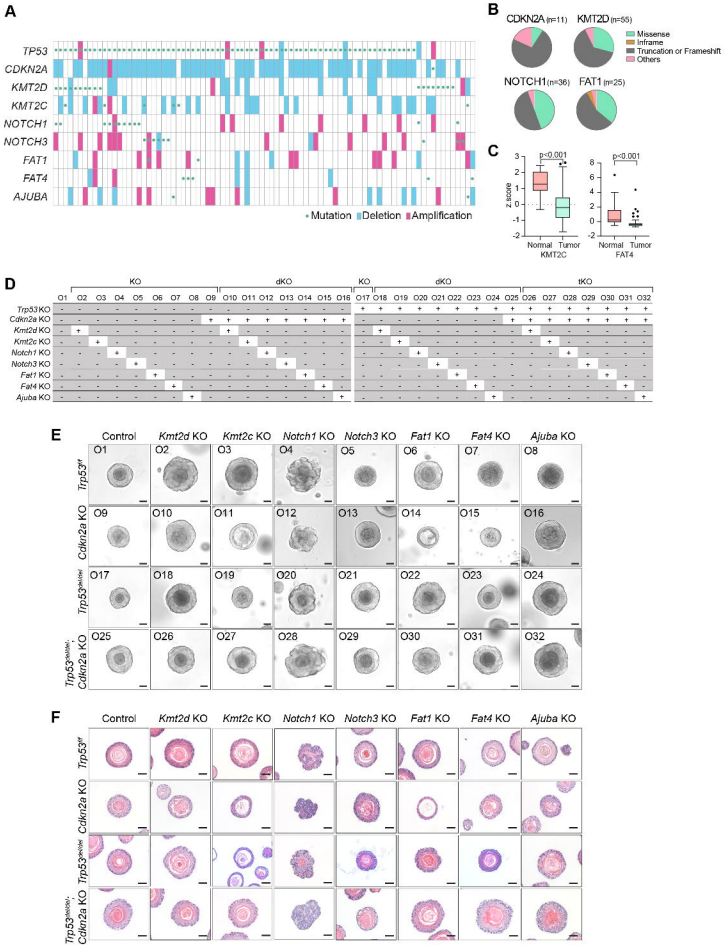
A
TP53
CDKN2A
KMT2D
KMT2C
NOTCH1
NOTCH3
FAT1
FAT4
AJUBA
Mutation
Deletion
Amplification
B
CDKN2A (n=11)
KMT2D (n=55)
NOTCH1 (n=36)
FAT1 (n=25)
Missense
Inframe
Truncation or Frameshift
Others
C
p<0.001
p<0.001
z.score
Normal
Tumor
KMT2C
FAT4
D
KO
dKO
KO
dKO
tKO
Trp53 KO
Cdkn2a KO
Kmt2d KO
Kmt2c KO
Notch1 KO
Notch3 KO
Fat1 KO
Fat4 KO
Ajuba KO
E
Control
Kmt2d KO
Kmt2c KO
Notch1 KO
Notch3 KO
Fat1 KO
Fat4 KO
Ajuba KO
Trp53tf
Cdkn2a KO
Trp53deletion
Cdkn2a KO
F
Control
Kmt2d KO
Kmt2c KO
Notch1 KO
Notch3 KO
Fat1 KO
Fat4 KO
Ajuba KO
Trp53tf
Cdkn2a KO
Trp53deletion
Cdkn2a KO

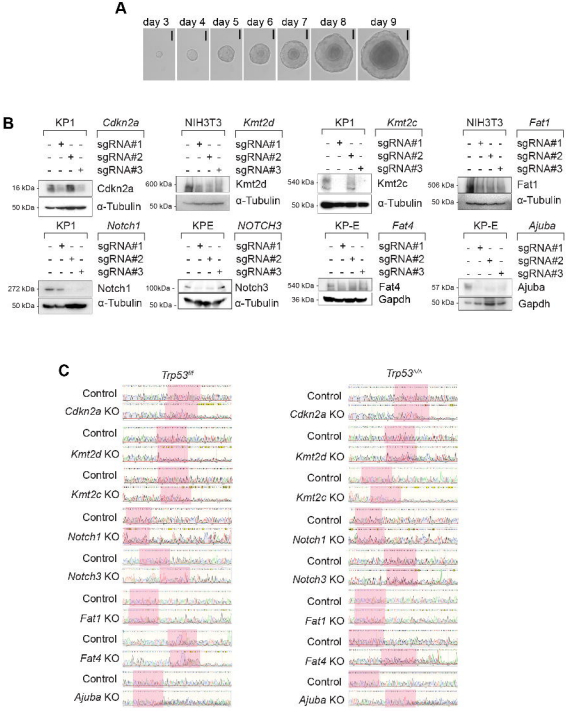
A
day 3
day 4
day 5
day 6
day 7
day 8
day 9
B
KP1
Cdkn2a
NIH3T3
Kmt2d
KP1
Kmt2c
NIH3T3
Fat1
sgRNA#1
sgRNA#2
sgRNA#3
16 kDa
50 kDa
Cdkn2a
α-Tubulin
600 kDa
50 kDa
Kmt2d
α-Tubulin
540 kDa
50 kDa
Kmt2c
α-Tubulin
506 kDa
50 kDa
Fat1
α-Tubulin
KP1
Notch1
KPE
NOTCH3
KP-E
Fat4
KP-E
Ajuba
272 kDa
50 kDa
Notch1
α-Tubulin
100kDa
50 kDa
Notch3
α-Tubulin
540 kDa
36 kDa
Fat4
Gapdh
57 kDa
50 kDa
Ajuba
Gapdh
C
Trp53fl/fl
Trp53Δ/Δ
Control
Cdkn2a KO
Control
Kmt2d KO
Control
Kmt2c KO
Control
Notch1 KO
Control
Notch3 KO
Control
Fat1 KO
Control
Fat4 KO
Control
Ajuba KO

Figure S3

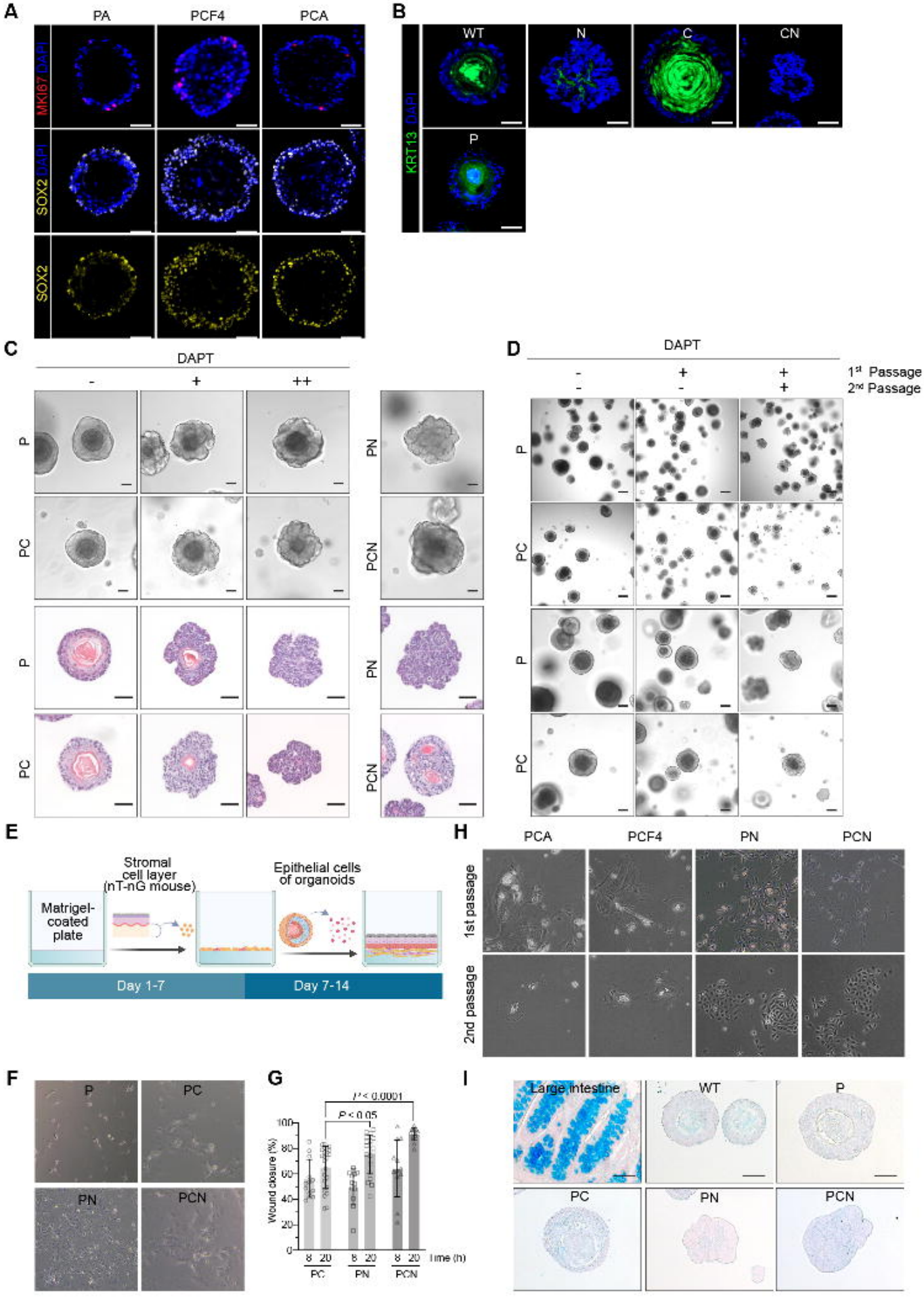
A
PA
PCF4
PCA
MKI67 DAPI
SOX2 DAPI
SOX2
B
WT
N
C
CN
P
KRT13 DAPI
C
DAPT
-
+
++
P
PC
PN
PCN
D
DAPT
1st Passage
2nd Passage
E
Stromal cell layer (nT-nG mouse)
Epithelial cells of organoids
Matrigel-coated plate
Day 1-7
Day 7-14
H
PCA
PCF4
PN
PCN
1st passage
2nd passage
F
P
PC
PN
PCN
G
P < 0.0001
P < 0.05
Wound closure (%)
Time (h)
PC
PN
PCN
I
Large intestine
WT
P
PC
PN
PCN

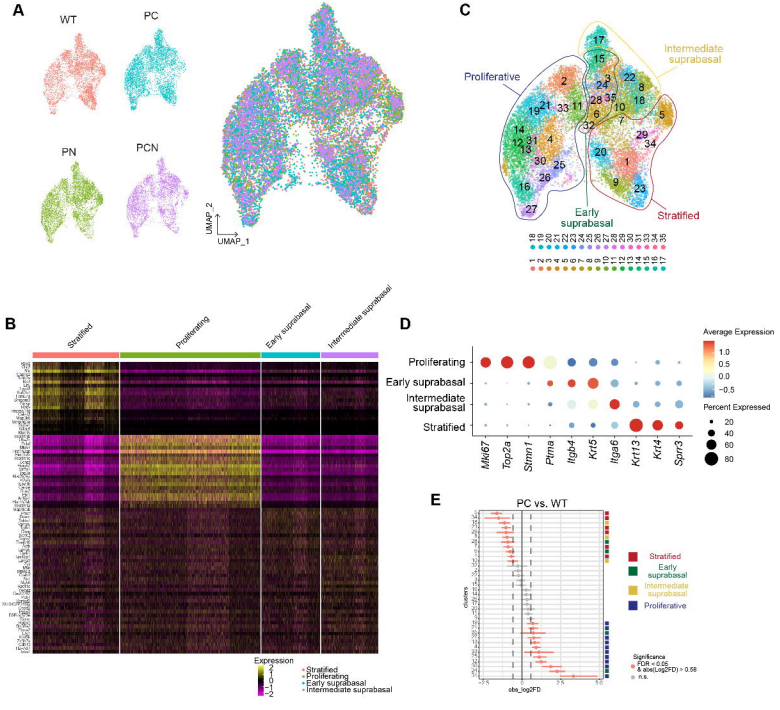
A
WT
PC
PN
PCN
UMAP_2
UMAP_1
C
Proliferative
Intermediate suprabasal
Early suprabasal
Stratified
B
Stratified
Proliferating
Early suprabasal
Intermediate suprabasal
Expression
Stratified
Proliferating
Early suprabasal
Intermediate suprabasal
D
Proliferating
Early suprabasal
Intermediate suprabasal
Stratified
Mki67
Top2a
Stmn1
Ptma
Itgb4
Krt5
Itga6
Krt13
Krt4
Sprr3
Average Expression
Percent Expressed
E
PC vs. WT
clusters
sbs_log2FD
Stratified
Early suprabasal
Intermediate suprabasal
Proliferative
Significance
FDR < 0.05
& abs(Log2FD) > 0.58
n.s.

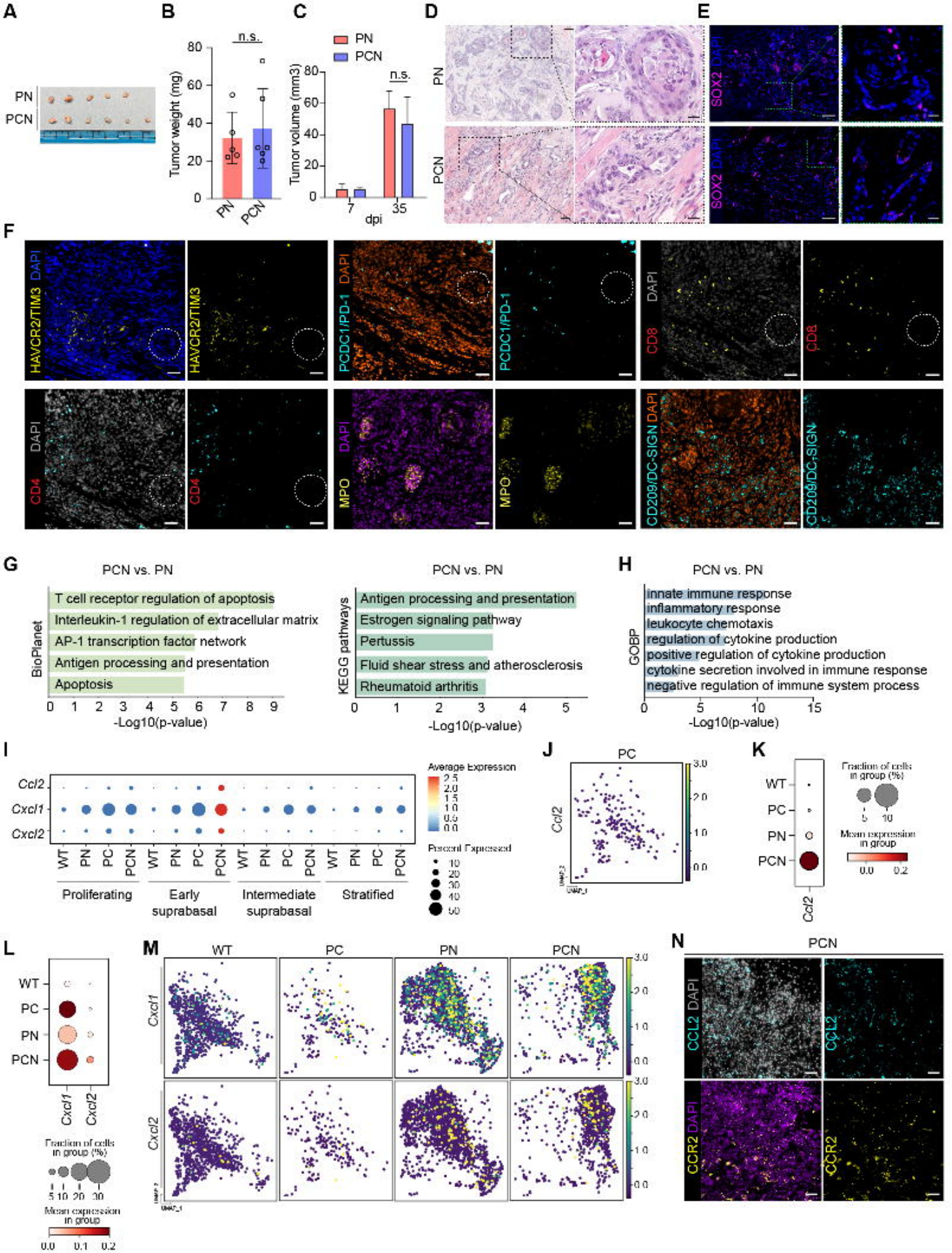
A
PN
PCN
B
n.s.
Tumor weight (mg)
PN
PCN
C
PN
PCN
n.s.
Tumor volume (mm3)
7
35
dpi
D
PN
PCN
E
SOX2 DAPI
F
HAVCR2/TIM3 DAPI
HAVCR2/TIM3
PCDC1/PD-1 DAPI
PCDC1/PD-1
CD8 DAPI
CD8
CD4 DAPI
CD4
MPO DAPI
MPO
CD209/DC-SIGN DAPI
CD209/DC-SIGN
G
PCN vs. PN
BioPlanet
T cell receptor regulation of apoptosis
Interleukin-1 regulation of extracellular matrix
AP-1 transcription factor network
Antigen processing and presentation
Apoptosis
-Log10(p-value)
PCN vs. PN
KEGG pathways
Antigen processing and presentation
Estrogen signaling pathway
Pertussis
Fluid shear stress and atherosclerosis
Rheumatoid arthritis
-Log10(p-value)
H
PCN vs. PN
GOBP
innate immune response
inflammatory response
leukocyte chemotaxis
regulation of cytokine production
positive regulation of cytokine production
cytokine secretion involved in immune response
negative regulation of immune system process
-Log10(p-value)
I
Ccl2
Cxcl1
Cxcl2
WT PN PC PCN
Proliferating
Early suprabasal
Intermediate suprabasal
Stratified
Average Expression
Percent Expressed
J
PC
Ccl2
K
WT
PC
PN
PCN
Ccl2
Fraction of cells in group (%)
Mean expression in group
L
WT
PC
PN
PCN
Cxcl1
Cxcl2
Fraction of cells in group (%)
Mean expression in group
M
WT
PC
PN
PCN
Cxcl1
Cxcl2
N
PCN
CCL2 DAPI
CCL2
CCR2 DAPI
CCR2

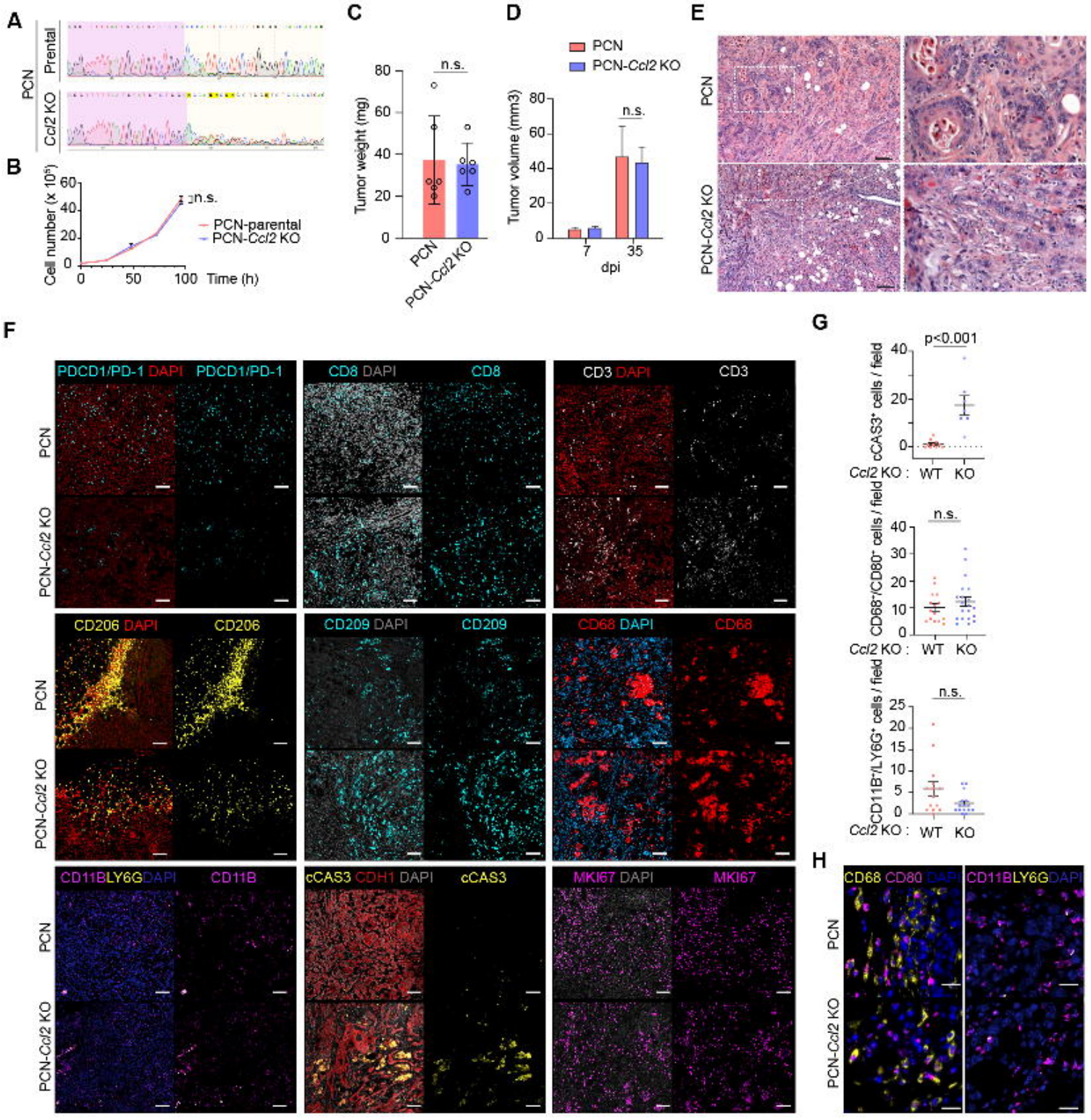
A
PCN
Prental
Ccl2 KO
B
Cell number (x 10⁵)
n.s.
PCN-parental
PCN-Ccl2 KO
Time (h)
C
Tumor weight (mg)
n.s.
PCN
PCN-Ccl2 KO
D
PCN
PCN-Ccl2 KO
Tumor volume (mm3)
n.s.
dpi
E
PCN
PCN-Ccl2 KO
F
PDCD1/PD-1 DAPI
CD8 DAPI
CD3 DAPI
CD206 DAPI
CD209 DAPI
CD68 DAPI
CD11BLY6G DAPI
cCAS3 CDH1 DAPI
MKI67 DAPI
G
p<0.001
cCAS3⁺ cells / field
n.s.
CD68⁺/CD80⁺ cells / field
n.s.
CD11B⁺/LY6G⁺ cells / field
Ccl2 KO : WT KO
H
CD68 CD80 DAPI
CD11BLY6G DAPI

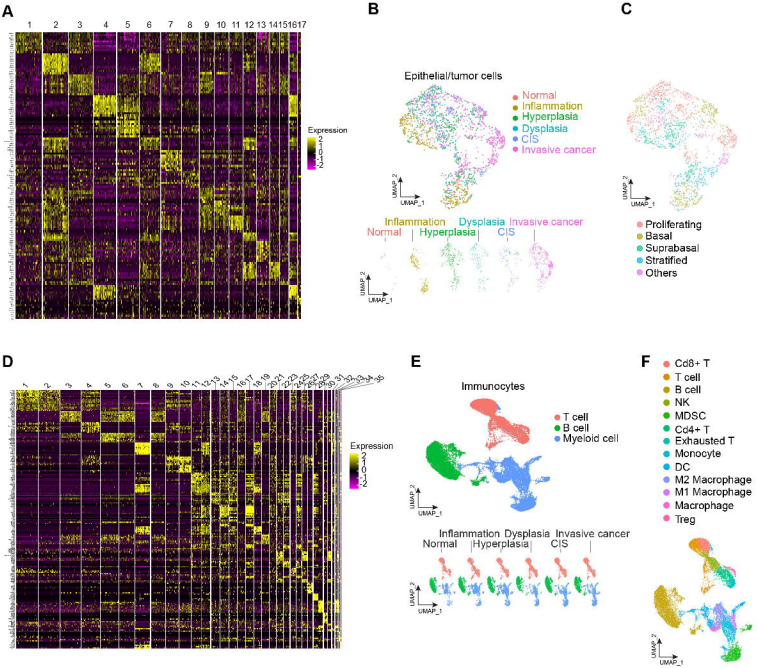
A
1 2 3 4 5 6 7 8 9 10 11 12 13 14 15 16 17
Expression
B
Epithelial/tumor cells
Normal
Inflammation
Hyperplasia
Dysplasia
CIS
Invasive cancer
UMAP_2
UMAP_1
Inflammation Dysplasia Invasive cancer
Normal Hyperplasia CIS
C
Proliferating
Basal
Suprabasal
Stratified
Others
D
Expression
E
Immunocytes
T cell
B cell
Myeloid cell
Inflammation Dysplasia Invasive cancer
Normal Hyperplasia CIS
F
Cd8+ T
T cell
B cell
NK
MDSC
Cd4+ T
Exhausted T
Monocyte
DC
M2 Macrophage
M1 Macrophage
Macrophage
Treg

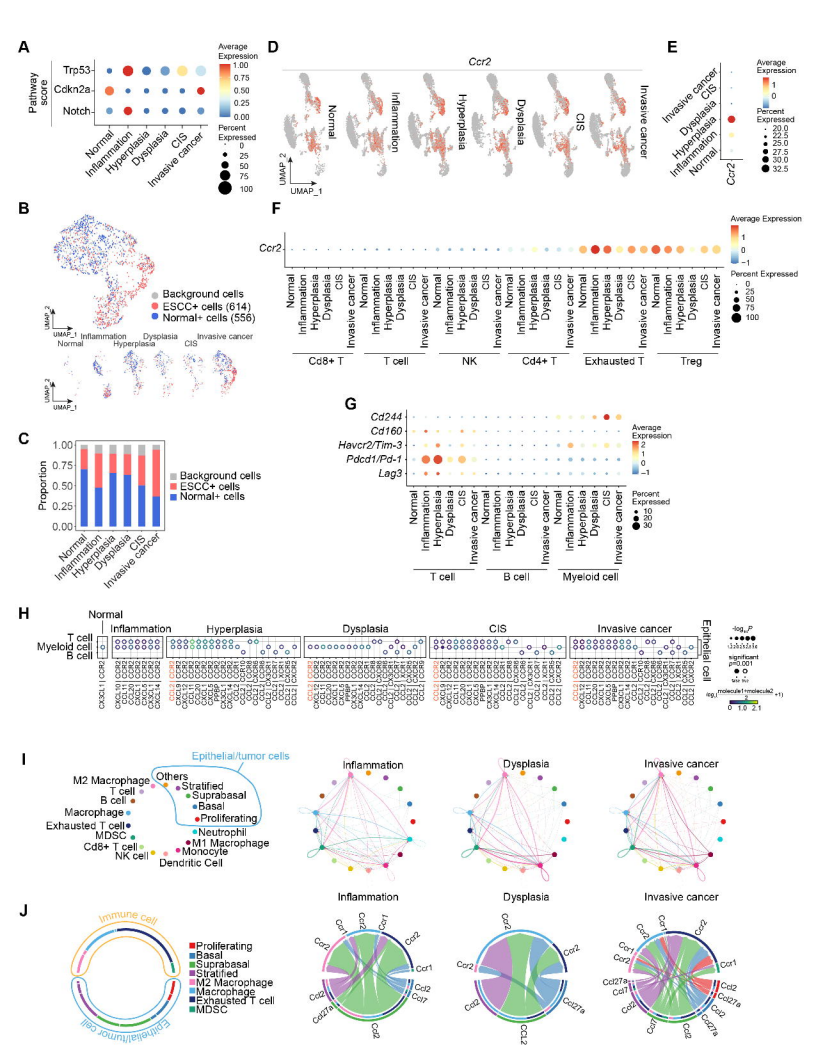
A
Pathway score
Trp53
Cdkn2a
Notch
Normal
Inflammation
Hyperplasia
Dysplasia
CIS
Invasive cancer
Average Expression
Percent Expressed
B
Background cells
ESCC+ cells (614)
Normal+ cells (556)
UMAP_1
UMAP_2
C
Proportion
Background cells
ESCC+ cells
Normal+ cells
D
Ccr2
Normal
Inflammation
Hyperplasia
Dysplasia
CIS
Invasive cancer
E
Ccr2
F
Ccr2
Cd8+ T
T cell
NK
Cd4+ T
Exhausted T
Treg
G
Cd244
Cd160
Havcr2/Tim-3
Pdcd1/Pd-1
Lag3
T cell
B cell
Myeloid cell
H
Normal
Inflammation
Hyperplasia
Dysplasia
CIS
Invasive cancer
T cell
Myeloid cell
B cell
Epithelial cell
I
Epithelial/tumor cells
M2 Macrophage
T cell
B cell
Macrophage
Exhausted T cell
MDSC
Cd8+ T cell
NK cell
Others
Stratified
Suprabasal
Basal
Proliferating
Neutrophil
M1 Macrophage
Monocyte
Dendritic Cell
Inflammation
Dysplasia
Invasive cancer
J
Immune cell
Epithelial/tumor cell
Proliferating
Basal
Suprabasal
Stratified
M2 Macrophage
Macrophage
Exhausted T cell
MDSC
Inflammation
Dysplasia
Invasive cancer

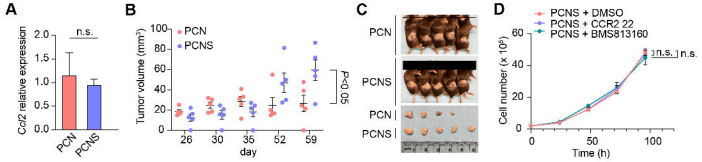
A
n.s.
Ccl2 relative expression
PCN
PCNS
B
PCN
PCNS
Tumor volume (mm³)
day
P<0.05
C
PCN
PCNS
D
PCNS + DMSO
PCNS + CCR2 22
PCNS + BMS813160
Cell number (x 10⁴)
Time (h)
n.s.
n.s.

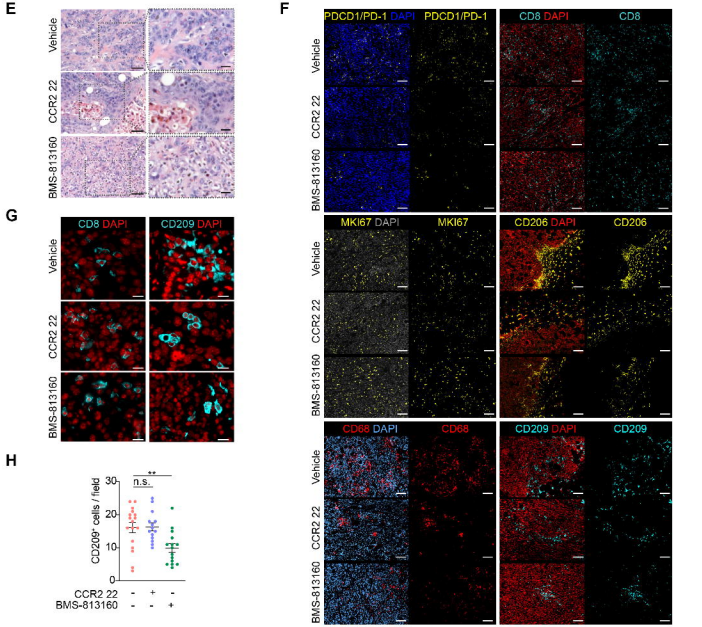
E
Vehicle
CCR2 22
BMS-813160
F
PDCD1/PD-1 DAPI
PDCD1/PD-1
CD8 DAPI
CD8
MKI67 DAPI
MKI67
CD206 DAPI
CD206
CD68 DAPI
CD68
CD209 DAPI
CD209
G
CD8 DAPI
CD209 DAPI
H
n.s.
**
CD209⁺ cells / field
CCR2 22
BMS-813160

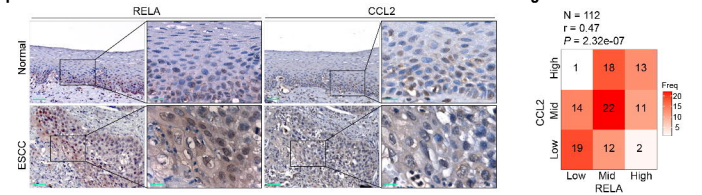
I
RELA
CCL2
Normal
ESCC
J
N = 112
r = 0.47
P = 2.32e-07
CCL2
High
Mid
Low
RELA
Low
Mid
High
Freq

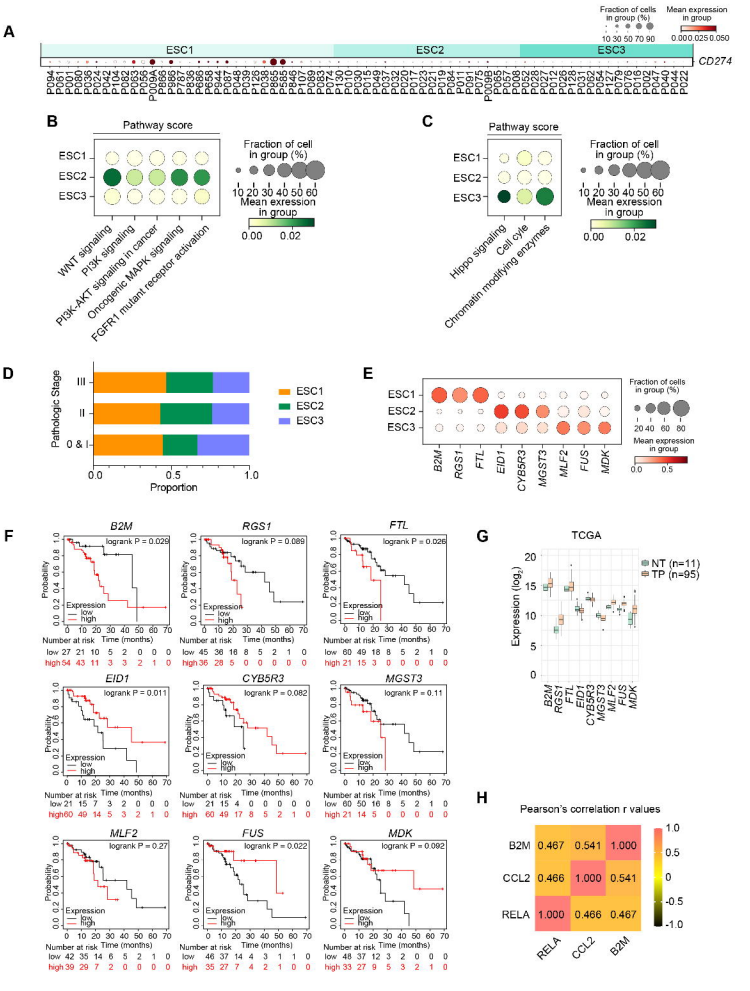
A
Fraction of cells in group (%)
10 30 50 70 90
Mean expression in group
0.000 0.025 0.050
ESC1
ESC2
ESC3
CD274
B
Pathway score
ESC1
ESC2
ESC3
WNT signaling
PI3K signaling
PI3K-AKT signaling in cancer
Oncogenic MAPK signaling
FGFR1 mutant receptor activation
Fraction of cell in group (%)
10 20 30 40 50 60
Mean expression in group
0.00 0.02
C
Pathway score
ESC1
ESC2
ESC3
Hippo signaling
Cell cyle
Chromatin modifying enzymes
Fraction of cell in group (%)
10 20 30 40 50 60
Mean expression in group
0.00 0.02
D
Pathologic Stage
III
II
0 & I
ESC1
ESC2
ESC3
0.0
0.5
1.0
Proportion
E
ESC1
ESC2
ESC3
B2M
RGS1
FTL
EID1
CYB5R3
MGST3
MLF2
FUS
MDK
Fraction of cells in group (%)
20 40 60 80
Mean expression in group
0.0 0.5
F
B2M
logrank P = 0.029
RGS1
logrank P = 0.089
FTL
logrank P = 0.026
EID1
logrank P = 0.011
CYB5R3
logrank P = 0.082
MGST3
logrank P = 0.11
MLF2
logrank P = 0.27
FUS
logrank P = 0.022
MDK
logrank P = 0.092
Probability
Expression
low
high
Time (months)
Number at risk
G
TCGA
NT (n=11)
TP (n=95)
Expression (log2)
B2M
RGS1
FTL
EID1
CYB5R3
MGST3
MLF2
FUS
MDK
H
Pearson's correlation r values
B2M 0.467 0.541 1.000
CCL2 0.466 1.000 0.541
RELA 1.000 0.466 0.467
RELA
CCL2
B2M
1.0
0.5
0
-0.5
-1.0